# Electronic structure of the 4*d* transition metal carbides: Dispersed fluorescence spectroscopy of MoC, RuC, and PdC

Ryan S. DaBell,[a] Raymond G. Meyer,[b] and Michael D. Morse[c]
*Department of Chemistry, University of Utah, Salt Lake City, Utah 84112*

(Received 31 May 2000; accepted 17 August 2000)

Dispersed fluorescence studies of the diatomic molecules MoC, RuC, and PdC are reported. New states identified in MoC and RuC are the $[\ldots]2\delta^1 12\sigma^1$, $^{3,1}\Delta_2$ states and the $[\ldots]2\delta^3 12\sigma^1$, $^1\Delta_2$ state, respectively. Five states are observed by dispersed fluorescence in PdC. The ground state is found to be $[\ldots]2\delta^4 12\sigma^2$, $^1\Sigma^+$, with the $[\ldots]2\delta^4 12\sigma^1 6\pi^1$, $^3\Pi_\Omega$ manifold of states lying about 2500 $cm^{-1}$ above the ground state. The $[17.9]\Omega=1$ state of PdC is also identified as $[\ldots]2\delta^4 12\sigma^1 13\sigma^1$, $^3\Sigma^+(\Omega=1)$, corroborating recent results of resonant two photon ionization spectroscopy studies. The spin-orbit interactions of these molecules are analyzed to deduce the composition of the molecular orbitals, and comparisons are made to *ab initio* theory when possible. An examination of the trends in bond energy, bond length, and vibrational frequency among the 4*d* transition metal carbides is also provided. © *2001 American Institute of Physics.*
[DOI: 10.1063/1.1316042]

## I. INTRODUCTION

The transition metal–carbon bond is of importance in such diverse fields as homogeneous and heterogeneous catalysis, organometallic chemistry, high temperature chemistry, materials science, and astrochemistry. Within the 4*d* series, the diatomic transition metal carbides have aroused considerable interest, beginning with spectroscopic studies of RuC[1,2] and RhC[3–6] in the late 1960's and early 1970's. Following a period of relative inactivity, the 4*d* transition metal carbides have received a flurry of spectroscopic attention in the last five years. This renewed interest stems in part from the recent discoveries that carbon nanotubes may be grown using small transition metal clusters as nucleation sites[7] and of the high stability of the metallocarbohedrene clusters $M_8C_{12}$.[8–12] Indeed, spectroscopic studies have now been published or reported in scientific meetings for every diatomic 4*d* transition metal carbide from YC to PdC, save TcC.[13–20] Much more is known of this series of molecules than of their analogs in the 3*d* series, where VC,[21,22] CoC,[22–24] FeC,[25–27] and NiC[28] have been investigated, or in the 5*d* series, where IrC[29–32] and PtC[33–37] have been examined. In addition, several theoretical studies of the 4*d* metal carbide series have been completed as well.[38–47]

The 4*d* transition metal carbides MoC, RuC, and PdC were recently characterized in this laboratory using resonant two-photon ionization (R2PI) spectroscopy.[13–15] These studies led to the determination of the ground states of MoC and RuC as $[\ldots]2\delta^2$, $^3\Sigma^-$, $\Omega=0^+$, and $[\ldots]2\delta^4$, $^1\Sigma^+$, respectively.[13,14] Most of the states of the $[\ldots]2\delta^3 6\pi^1$ configuration of RuC were observed and characterized as well.[14] Not all aspects of these studies were as productive, however. For instance, all spectroscopically observed states of MoC, except for the ground state, were found to possess $\Omega'=1$.[13] While interesting, this fact makes it rather difficult to deduce $\Lambda$-*S* terms for these states. A similar problem arose in the case of PdC, where the observation of an $\Omega=0$ ground state could be consistent with any of the three likely candidates: $[\ldots]2\delta^4 12\sigma^2$, $^1\Sigma^+(\Omega=0^+)$; $[\ldots]2\delta^4 12\sigma^1 6\pi^1$, $^3\Pi(\Omega=0)$; or $[\ldots]2\delta^4 6\pi^2$, $^3\Sigma^-(\Omega=0^+)$.[15] Because of this ambiguity, the ground state of the molecule could not be determined solely on the basis of the R2PI experiments. A desire to resolve this issue provided one of the reasons for the present study.

More fundamentally, the goal of this investigation is to establish a unified understanding of the electronic structure of the diatomic 4*d* transition metal carbides, particularly for the ground state and for states lying within 10 000 $cm^{-1}$ of the ground state. It is these states, or their analogues in polyatomic molecules, that are the most likely participants in catalytic processes involving the transition metal–carbon bond. As the metal–carbon interaction is the most basic aspect of organometallic chemistry, a thorough understanding of how these species interact at low energies is an essential prerequisite to increasing our knowledge of more complicated systems.

Section II of this paper provides a brief discussion of the experimental methods employed in the study, while Sec. III describes the detailed results obtained. In Sec. IV the effects of spin-orbit interactions in these molecules are considered, leading to an analysis of the atomic compositions of some of the molecular orbitals. Section IV also provides an examination of the trends in bond energy, bond length, and vibrational frequency among the 4*d* transition metal carbides. Section V then concludes the paper with a restatement of the most important results.

[a]Present Address: National Institute of Standards and Technology, 100 Bureau Dr., Gaithersburg, MD 20899-8393.
[b]Present Address: Department of Chemistry, University of Michigan, Ann Arbor, MI 48109.
[c]Electronic mail: morse@chemistry.chem.utah.edu

 

## II. EXPERIMENT

The instrument employed for these studies has been described previously.[48] In its original form the instrument used a monochromator and photomultiplier tube to record dispersed fluorescence spectra. These have now been replaced by a spectrograph and an intensified charge coupled device (CCD) camera. Details of the instrumental modifications are given below.

Reactive transition metal molecules were produced using the fundamental radiation of a Nd:YAG laser (10 mJ/pulse, focused to 0.5 mm diam) to ablate metal from a sample disk placed in the throat of a supersonic expansion of helium seeded with ~3% $CH_4$. The sample was rotated and translated using a system of gears and a camshaft to effect even removal of metal from the disk.[49] A custom-built dual-solenoid pulsed valve was used to pulse a flow of carrier gas over the metal sample from a reservoir held to approximately 80 psig. A supersonic expansion resulted when the gas expanded through a 2 mm orifice into a vacuum chamber that was held to a nominal operating pressure of $2\times10^{-4}$ Torr.

Approximately 0.5 cm past the exit orifice, the molecular beam was probed at right angles using radiation from a tunable dye laser pumped by the second or third harmonic of a second Nd:YAG laser. Fluorescence was collected perpendicular to both the molecular beam and the excitation dye laser beam; a first surface spherical mirror was placed below the collection point to increase the amount of light collected. The accumulated light was then collimated and imaged onto the entrance slit of a spectrograph. Within the spectrograph, the fluorescence was dispersed using one of three diffraction gratings (300 lines/mm, 1800 lines/mm, or 2400 lines/mm) before being imaged onto the detector head of a CCD camera that was thermoelectrically cooled to $-30\,^{\circ}C$, and kept dry using a flow of nitrogen at ~500 ml/min. The system was calibrated using known Hg, Ar, and Ne atomic lines emitted from hollow cathode tubes, as reported in the MIT wavelength tables.[50]

A microchannel plate at the head of the intensified CCD allowed detection to be gated in time using a commercial pulse generator. This was necessary to minimize false signals arising from macroscopic incandescent metallic objects that are produced in the laser ablation process; these commonly arrive in the viewing area at least 50 $\mu$s after the diatomic metal carbide molecules and other small clusters.[48] Typically, intensified CCD gate widths were set to ~2 $\mu$s, with the onset of the gate occurring 270 to 800 ns after the excitation laser pulse, depending on the fluorescence lifetime, the molecular concentration, and the severity of the scattered laser light problem.

Because laser ablation of a metal target in a stream of helium containing 3% $CH_4$ leads to the production of a wide variety of atoms and molecules, care was taken to verify that the observed emission signals originated from the molecule of interest. Previously collected R2PI spectra[13–15] of MoC, RuC, and PdC, and a previously collected RuC absorption spectrum[2] were used to select excitation wavelengths for these molecules. By comparing the relative frequencies of emission signals collected from each excitation band, it was a straightforward process to identify signals originating from the molecules of interest. Emissions due to other species can arise from two different processes. First, such data may result from one-photon excitation of a coincident transition in another small molecule that is present in the molecular beam. However, it is rare that transitions of a particular contaminating species overlap with more than one transition in the molecule of interest. Therefore, emissions arising from impurities are unlikely to be reproduced when exciting another band of the molecule of interest. Second, emission features may result from multiphoton absorption in polyatomic metal clusters, leading to production of fragments (particularly atoms) in excited electronic states. The resulting emission spectra generally display little dependence on the precise excitation frequency. Emissions of this type may be observed when several different bands are excited, but these signals are reproducible as a function of *absolute* wave number, as opposed to wave number relative to the excitation frequency. By keeping these two points in mind, it is straightforward to screen out data unrelated to the molecule under investigation. Having taken these precautions, it is reasonable to conclude that all dispersed fluorescence data presented in this work come exclusively from fluorescence of MoC, RuC, and PdC.

## III. RESULTS AND ANALYSIS

Dispersed fluorescence data were collected by exciting a total of 45 bands of MoC, RuC, and PdC that were initially observed using resonant two-photon ionization (R2PI) spectroscopy,[13–15] or by absorption spectroscopy.[2] Emission frequencies measured from different excitations were placed on a common relative scale by subtracting the excitation frequency ($\nu_{ex}$) from the emission frequency ($\nu_{em}$), resulting in data presented in relative wave numbers as $\nu_{rel}=\nu_{em}-\nu_{ex}$. As all values of $\nu_{rel}$ are less than 0 $cm^{-1}$, $-\nu_{rel}$ corresponds to the energy of a given vibrational level within a given electronic state. Vibrational levels within a given progression were identified; the average and standard deviation of each level were calculated using standard formulas. Using these data, the spectroscopic constants $T_0$, $\omega_e$, and $\omega_e x_e$ were derived using the expression

$$\nu_{rel}=-T_0-\omega_e v+\omega_e x_e(v^2+v), \tag{3.1}$$

where $T_0$ gives the energy of the $v=0$ level relative to the $v=0$ level of the ground state.

Rotational contours of the fluorescence bands were also used to deduce $\Omega''$ values of the lower states. While the resolution of the experiment (typically 1.5–5 $cm^{-1}$) was insufficient to fully resolve rotational lines, it was sufficient to establish the relative intensities of *P*-, *Q*-, and *R*-branches when the total intensity of the emission was sufficiently strong. By comparing these branch intensities with the predictions of the Hönl–London formulas,[51] it was possible to determine the value of $\Omega''$. This, in turn, allowed the lower state $\Lambda$-*S* term to be deduced.

To clarify the electronic states of the $4d$ transition metal carbides, a qualitative molecular orbital diagram for the MoC, RuC, and PdC, molecules is presented in Fig. 1. This diagram implicitly assumes that the states of interest are well-described by single-configuration wave functions, and that the orbital energies do not change significantly when the

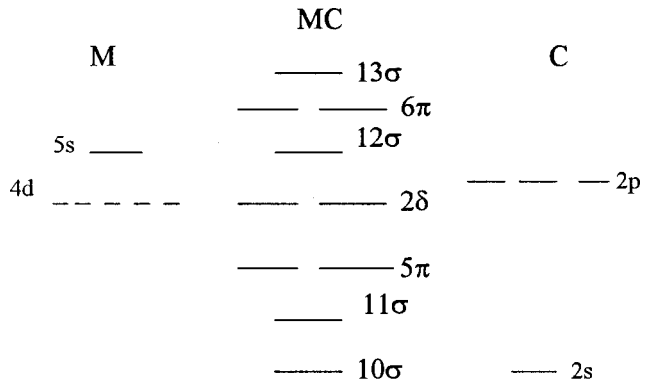


FIG. 1. Qualitative molecular orbital (MO) diagram for the diatomic $4d$ transition metal carbides.

orbital occupations are changed. Further, by applying the same diagram to MoC, RuC, and PdC, it is assumed that the relative energies of the molecular orbitals change rather little as one moves across the $4d$ series. Of course, these assumptions cannot be completely valid. Nevertheless, this molecular orbital diagram is useful for understanding the general electronic structure of these molecules.

The $10\sigma$ orbital is comprised mainly of the $2s$ orbital of carbon, and is generally considered to be corelike. The $11\sigma$ and $5\pi$ orbitals are bonding combinations of the $|m_l|=0$ and 1 components, respectively, of the metal $4d$ and carbon $2p$ orbitals; their antibonding counterparts are the $13\sigma$ and $6\pi$ orbitals, respectively. The nonbonding $2\delta$ orbitals are essentially pure metal $4d\,\delta$ orbitals, because of the lack of low-lying $\delta$ orbitals on carbon. The $12\sigma$ orbital is composed mainly of the metal $5s$ orbital, and is generally nonbonding in character. Hyperfine splitting observed in the spectrum of RuC, for example, has demonstrated that the $12\sigma$ orbital is approximately 83% ruthenium $5s$ in character.[14] Estimates of the atomic orbital contributions to these molecular orbitals, as deduced from the present experiments, are presented in detail in Sec. IV.

### A. MoC

Dispersed fluorescence spectra were collected from 17 excitation bands of MoC that were originally observed in this laboratory using resonant two-photon ionization (R2PI) spectroscopy. Table I gives the emission bands observed from various excitations of MoC. Table II lists the vibronic levels deduced from the dispersed fluorescence experiments, along with the results of a fit of these levels to obtain the spectroscopic constants $T_0$, $\omega_e''$, and $\omega_e''x_e''$.

All of the excited states known for MoC have $\Omega'=1$.[13] Under electric dipole selection rules, emission from an $\Omega'=1$ state is allowed to states of $\Omega''=0^+$, $0^-$, 1, or 2. Thus emission to the $v''=0-3$ vibrational levels of the ground $X\,^3\Sigma_{0^+}^-$ state are observed following the excitations listed in Table I. Emission to the $X\,^3\Sigma_1^-$ state, predicted to lie approximately 155 $\mathrm{cm}^{-1}$ above the $\Omega=0^+$ level,[13] could not be observed. This suggests that the projection of spin on the internuclear axis, $\Sigma$, remains a good quantum number in all of the excited states probed in this experiment. Because $\Sigma=0$ in the $X\,^3\Sigma_{0^+}^-$ state, this further suggests that all of the known excited levels of MoC, which have $\Omega'=1$, are $\Pi$ states.

TABLE I. Dispersed fluorescence excitation and emission bands of MoC.

| Excitation | | | Levels observed in emission: | | |
|---|---|---|---|---|---|
| Band system[a] | $\nu_0$[b] | $v'-v''$ | $X\,^3\Sigma^-$ | $[4.0]^3\Delta_2$ | $[7.8]^1\Delta_2$ |
| $[18.6]\Omega'=1-X\,^3\Sigma_{0+}^-$ | 18 611.9526 | 0-0 | 0-3 | 0-2 | |
| | 19 453.0364 | 1-0 | 0-2 | 0 | |
| $[20.70]\Omega'=1-X\,^3\Sigma_{0+}^-$ | 20 699.6868 | 0-0 | 0, 2, 3 | 0, 2 | 0 |
| | 21 538.1524 | 1-0 | 0-2 | 1 | |
| $[22.5]\Omega'=1-X\,^3\Sigma_{0+}^-$ | 22 520.3665 | 0-0 | 0-2 | 0-2 | 0 |
| | 23 323.5623 | 1-0 | 0, 1 | 0-2 | 0, 1 |
| $\Omega'=1-X\,^3\Sigma_{0+}^-$ | 19 344.7021[c] | | 0-3 | 0 | |
| $\Omega'=1-X\,^3\Sigma_{0+}^-$ | 20 094.4379 | | 0, 1 | 0, 1 | |
| $\Omega'=1-X\,^3\Sigma_{0+}^-$ | 20 862.99 | | 0, 1 | 1 | |
| $\Omega'=1-X\,^3\Sigma_{0+}^-$ | 20 901.6829 | | 0, 1 | 1 | |
| $\Omega'=1-X\,^3\Sigma_{0+}^-$ | 21 233.9928 | | 0, 1 | 0, 1 | |
| $\Omega'=1-X\,^3\Sigma_{0+}^-$ | 21 389.66 | | 0, 1 | 1 | |
| $\Omega'=1-X\,^3\Sigma_{0+}^-$ | 22 338.281 | | 0, 1, 3 | 1, 2 | 0 |
| $\Omega'=1-X\,^3\Sigma_{0+}^-$ | 22 348.3627 | | 0, 2 | 2 | 0, 1 |
| $\Omega'=1-X\,^3\Sigma_{0+}^-$ | 22 844.5200 | | 0-2 | 2 | |
| $\Omega'=1-X\,^3\Sigma_{0+}^-$ | 22 968.22 | | 0, 3 | | |
| $\Omega'=1-X\,^3\Sigma_{0+}^-$ | 22 992.78 | | 0 | 1 | |

[a]Band systems are designated as described in Ref. 13, with the number in square brackets providing the energy of the $v=0$ level, in thousands or $\mathrm{cm}^{-1}$.

[b]$\nu_0$ provides the band origin of the excitation band for $^{98}$Mo $^{12}$C, in $\mathrm{cm}^{-1}$ (see Ref. 13). The actual excitation wave number employed was adjusted to maximize the fluorescence signal and typically fell within 5 $\mathrm{cm}^{-1}$ of $\nu_0$.

[c]$\nu_0$ for $^{98}$Mo $^{12}$C is not known for this band. $\nu_0$ for $^{96}$Mo $^{12}$C is reported from Ref. 13.

TABLE II. Vibronic levels of MoC and fitted spectroscopic constants.

| Electronic state | $v$ | Energy ($cm^{-1}$)[a] | Fitted energy ($cm^{-1}$) | Residual ($cm^{-1}$) |
|---|---|---|---|---|
| $X\,^3\Sigma^-_{0+}$ | 0 | 0.00 | 0.00 | 0.00 |
| | 1 | 1000.42(4.00) | 1001.66 | −1.24 |
| | 2 | 1997.70(3.62) | 1996.68 | 1.01 |
| | 3 | 2984.10(6.05) | 2985.05 | −0.94 |
| $[4.0]^3\Delta_2$ | 0 | 4002.50(3.73) | 4002.50 | 0.00 |
| | 1 | 5002.80(4.54) | 5002.80 | 0.00 |
| | 2 | 6000.40(4.21) | 6000.40 | 0.00 |
| $[7.8]^1\Delta_2$ | 0 | 7834.2(2.7) | -- | -- |
| | 1 | 8865.3(8.5) | -- | -- |

Fitted spectroscopic constants

| Electronic state | $T_0$($cm^{-1}$)[b] | $\omega_e$ ($cm^{-1}$)[b] | $\omega_e x_e$ ($cm^{-1}$)[b] |
|---|---|---|---|
| $[7.8]^1\Delta_2$ | 7834.2(2.7) | $\Delta G_{1/2}$= 1031(9) | |
| $[4.0]^3\Delta_2$ | 4002.5(3.7) | 1003(16) | 1.4(5.3) |
| $X\,^3\Sigma^-_{0+}$ | 0 | 1008.3(6.7) | 3.3(2.0) |

[a]Numbers in parentheses represent $1\sigma$ error estimates of the averaged data, in $cm^{-1}$.

[b]Numbers in parentheses provide $1\sigma$ error estimates of the propagated errors, in $cm^{-1}$. $T_0$ of the $X\,^3\Sigma^-_{0+}$ state is constrained to be identically zero, and is without error.

### 1. The $[4.0]^3\Delta_2$ state

In addition to fluorescence to the $X\,^3\Sigma^-_{0+}$ ground state, fluorescence to another electronic state with $T_0 \sim 4000\,cm^{-1}$ was also observed. In Fig. 2, the band contours of the emission from the $v=0$ level of the $[18.6]\Omega=1$ state to the $v=0$ levels of the $X\,^3\Sigma^-_{0+}$ ground state (upper panel) and of the new state near 4000 $cm^{-1}$ (lower panel) are compared. Because of the small isotope shift in the $[18.6]\Omega=1\leftarrow X\,^3\Sigma^-_{0+}$ 0-0 excitation,[13] excitation of this band provides the best opportunity to observe the rotational profiles of these emission bands, which are also expected to have small isotope shifts due to their vibrational assignment as 0-0 bands. For the $[18.6]\Omega=1\rightarrow X\,^3\Sigma^-_{0+}$ emission displayed in the upper panel, a strong $R$-branch, moderately intense $Q$-branch, and weak $P$-branch are observed. According to the Hönl–London formulas,[51] this is precisely what is expected for an $\Omega'=1\rightarrow\Omega''=0$ emission. In contrast, fluorescence to the state near 4000 $cm^{-1}$ (lower panel), displays much greater intensity in the $P$-branch than in the $R$-branch. Again, following the Hönl–London formulas,[51] this is what is expected for an $\Omega'=1\rightarrow\Omega''=2$ emission.

In assigning a $\Lambda$-$S$ term to the $[4.0]\Omega=2$ state observed here, one should realize that no states with $\Omega=2$ derive from the $[\ldots]10\sigma^2 5\pi^4 11\sigma^2 2\delta^2$ ground electronic configuration. Thus we must consider low-lying excited electronic configurations for the $[4.0]\Omega=2$ state. A likely choice for this configuration is $[\ldots]2\delta^1 12\sigma^1$, where one electron has been promoted from the nonbonding $2\delta$ orbital to the nonbonding $12\sigma$ orbital. The $[\ldots]2\delta^1 12\sigma^1$ configuration is expected to produce lower-lying excited states than any of the other possible configurations, such as the $[\ldots]2\delta^1 6\pi^1$ or $[\ldots]5\pi^3 2\delta^2 12\sigma^1$, that involve the promotion of an electron from a nonbonding orbital to an antibonding orbital, or from a bonding orbital to a nonbonding orbital, respectively. Indeed, the $^3\Pi_1$ state of the $[\ldots]5\pi^3 2\delta^2 12\sigma^1$ configuration is thought to provide much of the oscillator strength for the excited states with $\Omega'=1$ that have been observed,[13] and which are excited in the present dispersed fluorescence study. Decay of the $[\ldots]5\pi^3 2\delta^2 12\sigma^1$, $^3\Pi_1$ state by relaxation of a $2\delta$ electron to the $5\pi$ orbital would result in allowed emission to the $[\ldots]2\delta^1 12\sigma^1$, $^3\Delta_2$ state; relaxation of the $12\sigma$ electron to the $5\pi$ orbital results in emission to the ground $[\ldots]5\pi^4 2\delta^2$, $X\,^3\Sigma^-_{0+}$ state. On this basis, the $\Omega=2$ state near 4000 $cm^{-1}$ is assigned as the $[\ldots]2\delta^1 12\sigma^1$, $^3\Delta_2$ state.

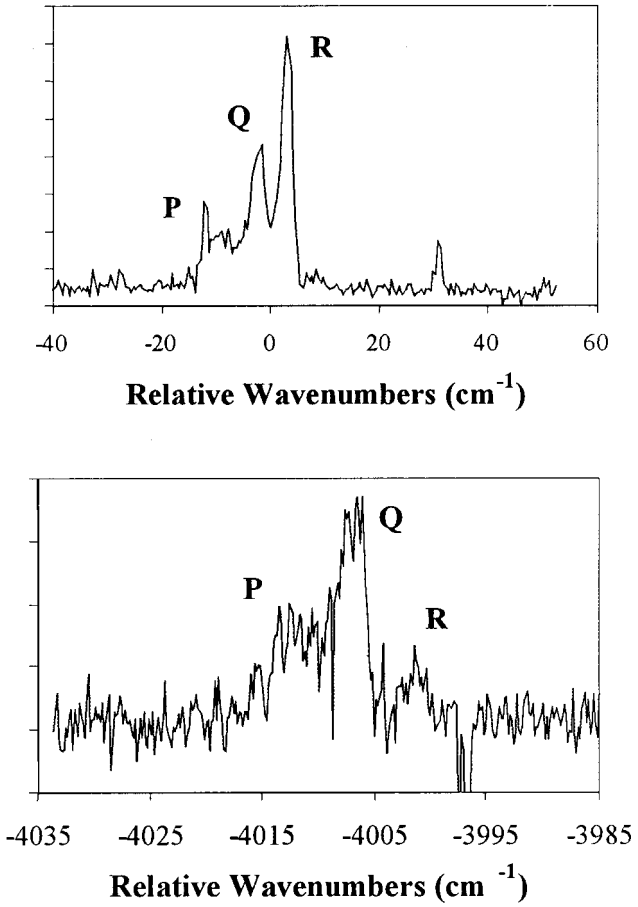


FIG. 2. Rotational band contour obtained by dispersed fluorescence of the 0-0 band of the $[18.6]\Omega'=1\rightarrow X\,^3\Sigma^-(0^+)$ system of MoC (upper panel), compared to the 0-0 band of the $[18.6]\Omega'=1\rightarrow[4.0]^3\Delta_2$ system (lower panel).

### 2. The $[7.8]^1\Delta_2$ state

Another electronic state, lying 7834 $cm^{-1}$ above the ground state, is observed in the dispersed fluorescence from five different excitations. Emission to this excited state is quite weak in intensity, approximately a factor of 10–20 weaker than the emission to the $^3\Delta_2$ state. This probably indicates a transition that is forbidden under Hund's case (a) selection rules, made allowed by spin-orbit interaction.

In considering the $\Lambda$-$S$ parentage of this electronic state, a likely candidate is the $[\ldots]2\delta^1 12\sigma^1$, $^1\Delta_2$ state. Although the intensity of the observed emission is too weak to allow the relative intensities of the rotational branches to be determined, and the $\Omega''$-value is therefore unknown, the vibrational interval of $\Delta G_{1/2}$= 1031 $cm^{-1}$ determined for this state is quite close to the value of $\Delta G_{1/2}$= 1000 $cm^{-1}$ obtained for

TABLE III. Dispersed fluorescence excitation and emission bands in RuC.

| Excitation | | | Levels observed in emission: | | | |
|---|---|---|---|---|---|---|
| Band system[a] | $\nu_0$[b] | $v'-v''$ | $X\,^1\Sigma^+$ | $[5.7]^1\Delta_2$ | $[0.1]^3\Delta_3$ | $[0.9]^3\Delta_2$ |
| $[12.7]\Omega'=2-{}^3\Delta_3$ | 14 582.7637 | 2-0 | | | 0-3 | |
| $[13.5]\Omega'=3-{}^3\Delta_3$ | 14 338.8389 | 1-0 | | | 0 | 0-2 |
| $[13.9]\Omega'=1-X\,^1\Sigma^+$ | 14 999.6904 | 2-0 | | | | 1.2 |
| $[16.2]\Omega'=3-{}^3\Delta_3$ | 16 119.1952 | 0-0 | | | | 0 |
| | 17 038.0407 | 1-0 | | 0 | | 0.1 |
| $[18.0]^1\Pi-X\,^1\Sigma^+$ | 18 086.0157 | 0-0 | 0-2 | 0-1 | | 0 |
| | 18 961.5391 | 1-0 | 0-5 | 0-2 | | 0 |
| | 19 828.3 | 2-0 | 0-5 | 0, 1 | | |
| | 20 684.4 | 3-0 | 0, 1, 3, 5 | 1, 2 | | |
| 4317 Å | 23 152.00 | 0-0 | | | 0-4 | |
| | 23 895.25 | 1-0 | | | 0-6 | |
| 4337 Å | 23 802.00 | 1-0 | | | 0-5, 7-9 | |
| 4383 Å | 23 578.50 | 1-0 | | | 0, 2-5 | 0-4 |

[a]Band systems from Ref. 14 are designated as described therein, with the number in square brackets providing the energy of the $v=0$ level, in thousands of $cm^{-1}$. Band systems from Ref. 2 are designated as described therein, using the wavelength position of the band head in Angstroms.

[b]$\nu_0$ provides the band origin of the excitation band for $^{102}Ru\,^{12}C$, in $cm^{-1}$ (Ref. 2, 14). The actual excitation wave number employed was adjusted to maximize the fluorescence signal and typically fell within 5 $cm^{-1}$ of $\nu_0$. The $[18.0]^1\Pi-X\,^1\Sigma^+$, 2-0 and 3-0 bands were found by extrapolation from the 0-0 and 1-0 bands reported previously. $\nu_0$ reported for these bands is the experimentally located position of maximum fluorescence intensity.

the $[4.0]\,^3\Delta_2$ state. The agreement between these two values suggests that the two states derive from the same configuration. Further, the weak intensity of the emission to this state suggests a spin-forbidden transition, as would be the case for a $[\ldots]5\pi^3 2\delta^2 12\sigma^1,\ ^3\Pi_1 \rightarrow [\ldots]2\delta^1 12\sigma^1,\ ^1\Delta_2$ emission process. Such an emission could be induced by spin-orbit mixing of $[\ldots]5\pi^3 2\delta^2 12\sigma^1,\ ^1\Pi_1$ character into the upper state or of $[\ldots]2\delta^1 12\sigma^1,\ ^3\Delta_2$ character into the lower state. In addition to these considerations, theoretical calculations, discussed below, also support the identification of this state as $[\ldots]2\delta^1 12\sigma^1,\ ^1\Delta_2$.[52]

#### 3. Comparison to theoretical calculations and other experiments

In the recent theoretical study of MoC by Shim and Gingerich,[52] it was calculated that the ground state of MoC is $[\ldots]5\pi^4 2\delta^2,\ ^3\Sigma^-(\Omega=0^+)$, with the $[\ldots]2\delta^1 12\sigma^1,\ ^3\Delta$ and $^1\Delta$ states lying at 4500 $cm^{-1}$ and 9312 $cm^{-1}$, respectively. The vibrational frequencies of these states are predicted to be 971 $cm^{-1}$ for $X\,^3\Sigma^-$, 1013 $cm^{-1}$ for $^3\Delta$, and 1026 $cm^{-1}$ for $^1\Delta$. The good agreement between these calculated values and our experimental values provides strong support for the assignments given here. These assignments are also in partial agreement with assignments provided in a recent photoelectron investigation of MoC.[17] In the photoelectron study, the $X\,^3\Sigma^-$ state is found to have a vibrational frequency of $1000\pm100\,cm^{-1}$, and the $^3\Delta_2$ state is found to lie at $4080\pm160\,cm^{-1}$, in good agreement with the present work. However, the $^1\Delta_2$ state was assigned as lying at $7240\pm80\,cm^{-1}$, with a vibrational frequency of $890\pm60\,cm^{-1}$.[17] These values are not in agreement with the present work, and either represent another electronic state of MoC or possibly correspond to another molecule entirely.

### B. RuC

Dispersed fluorescence was observed by exciting 13 bands of RuC that were originally observed by emission[1,2] and R2PI[14] spectroscopies. Vibrational progressions were observed in the $X\,^1\Sigma^+$, $[0.1]^3\Delta_3$, $[0.9]^3\Delta_2$, and $[5.7]^1\Delta_2$ states of RuC. To place the data on a common energy scale, vibrational levels observed via excitation from the $[0.1]^3\Delta_3$, $v=0$ lower state were shifted by 75.953 $cm^{-1}$, the known energy of the $[0.1]^3\Delta_3$, $v=0$ level.[14] This is the first observation of the $[5.7]^1\Delta_2$ state, and justification for its assignment is given below. A list of the bands excited and the resulting emission bands is found in Table III. The vibronic levels identified from this work are given in Table IV, and a compilation of the states and spectroscopic constants currently known for this molecule is provided in Table V.

#### 1. Observation of the $[5.7]\,^1\Delta_2$ state

In dispersed fluorescence from the $[18.0]\,^1\Pi$ state, emissions to vibrational levels in the $X\,^1\Sigma^+$ state, the $[0.9]\,^3\Delta_2$ state, and a state near 5679 $cm^{-1}$ were observed. Dispersed fluorescence spectra of the emissions from the $[18.0]\,^1\Pi$, $v=0$ level to the $X\,^1\Sigma^+$, $v=0$ level (upper panel) and to the $v=0$ level of the state near 5679 $cm^{-1}$ (lower panel) are displayed in Fig. 3. Because fluorescence to both states originates from the $[18.0]\,^1\Pi$ state, $\Omega'=1$ for both emission bands. Fluorescence to the $X\,^1\Sigma^+$ ground state is an $\Omega'=1\rightarrow\Omega''=0$ emission, and is expected to display greater intensity in the *R*-branch than in the *P*-branch, according to the Hönl–London formulas.[51] This is the pattern of branch intensities observed in the upper panel of Fig. 3.

The lower panel of Fig. 3 displays the dispersed fluorescence to the $v=0$ level of the new state near 5679 $cm^{-1}$. In contrast to the emission to the ground state, this band dis-

TABLE IV. Vibronic levels of RuC and fitted spectroscopic constants.

| Electronic state | $v$ | Energy[a] ($cm^{-1}$) | Fitted energy ($cm^{-1}$) | Residual ($cm^{-1}$) |
|---|---|---|---|---|
| $^1\Sigma^+$ | 0 | 0.00 | 0.00 | 0.00 |
| | 1 | 1088.0(2.39) | 1089.3 | −1.3 |
| | 2 | 2167.7(1.85) | 2167.8 | −0.1 |
| | 3 | 3236.8(1.36) | 3235.7 | 1.1 |
| | 4 | 4292.9(0.14) | 4292.9 | −0.0 |
| | 5 | 5346.1(6.10) | 5339.4 | 6.7 |
| $^3\Delta_3$ | 0 | 75.953[b] | 76.996 | −1.043 |
| | 1 | 1105.7(0.47) | 1105.9 | −0.2 |
| | 2 | 2123.3(4.22) | 2124.6 | −1.3 |
| | 3 | 3136.3(5.59) | 3133.8 | 2.5 |
| | 4 | 4130.4(5.16) | 4133.3 | −2.9 |
| | 5 | 5125.0(7.88) | 5123.0 | 2.0 |
| | 6 | 6108.8(2.0) | 6103.2 | 5.6 |
| | 7 | 7072.0(2.0) | 7073.5 | −1.4 |
| | 8 | 8064.4(2.0)[c] | | |
| | 9 | 8984.1(2.0) | 8985.1 | −1.0 |
| $^3\Delta_2$ | 0 | 845.5(3.55) | 845.2 | 0.3 |
| | 1 | 1873.0(7.64) | 1876.0 | −3.0 |
| | 2 | 2896.6(5.52) | 2895.3 | 1.3 |
| | 3 | 3902.6(2.0) | 3903.1 | −0.5 |
| | 4 | 4899.1(2.0) | 4899.5 | −0.4 |
| $^1\Delta_2$ | 0 | 5679.13(1.15) | 5679.13 | 0.00 |
| | 1 | 6735.03(2.88) | 6735.03 | 0.00 |
| | 2 | 7778.55(5.02) | 7778.55 | 0.00 |
| $[18.0]^1\Pi_1$ | 0 | 18 087.5(2.0) | 18 088.2 | −0.7 |
| | 1 | 18 967.5(2.0) | 18 965.3 | 2.2 |
| | 2 | 19 828.3(2.0) | 19 830.5 | −2.2 |
| | 3 | 20 684.4(2.0) | 20 683.7 | 0.7 |

[a]Numbers in parentheses provide $1\sigma$ error estimates of the averaged data, in $cm^{-1}$. If the vibrational level was observed from emission in only one band, an error estimate of 2.0 $cm^{-1}$ is used.
[b]Observed $^3\Delta_3$ and $^3\Delta_2$ progressions from $^3\Delta_3$ excitation bands were shifted by 75.953 $cm^{-1}$, the difference between $T_0(X\,^1\Sigma^+)$ and $T_0(^3\Delta_3)$ as reported in Ref. 14.
[c]Omitted from fit.

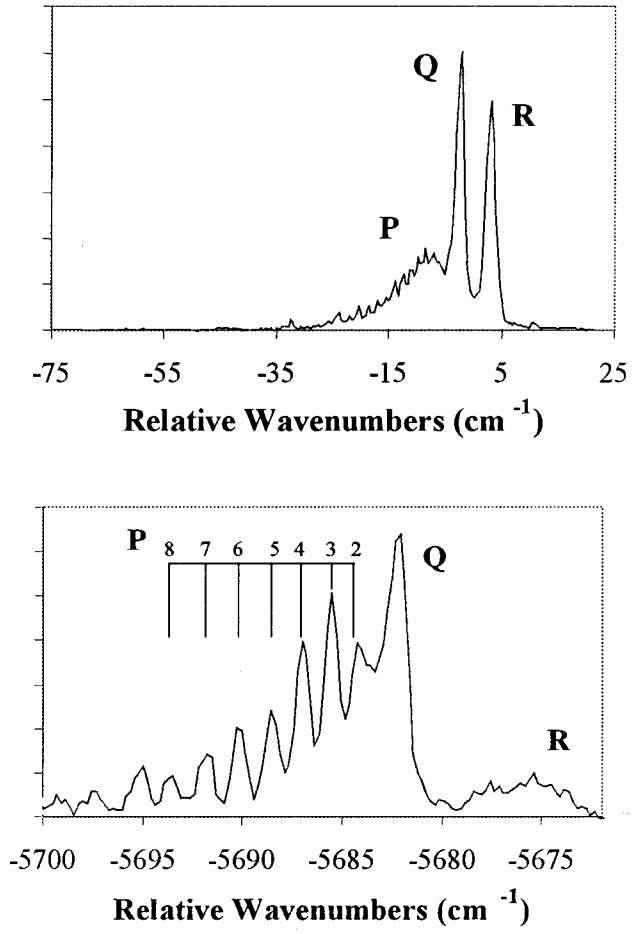


FIG. 3. Rotational band contour obtained by dispersed fluorescence of the 0-0 band of the $[18.1]^1\Pi_1 \rightarrow X\,^1\Sigma^+$ system of RuC (upper panel), compared to the 0-0 band of the $[18.1]^1\Pi_1 \rightarrow [5.7]^1\Delta_2$ system (lower panel). Rotational lines of the $P$-branch are partially resolved, giving $B_0(^1\Delta_2) = 0.5964 \pm 0.0004$ $cm^{-1}$.

TABLE V. Fitted spectroscopic constants of RuC.[a]

| State | $T_0$ ($cm^{-1}$)[b] | $\omega_e$ ($cm^{-1}$)[b] | $\omega_e x_e$ ($cm^{-1}$)[b] | $B_e$ ($cm^{-1}$)[b] | $r_e$ (Å)[b] |
|---|---|---|---|---|---|
| $[18.1]^1\Pi_1$ | 18 086.016[c] | 889.0(6.7) | 6.0(1.6) | 0.557 343[c] | 1.678 50[c] |
| $[16.2]^1\Phi_3$ | 16 195.145[c] | $\Delta G_{1/2} = 918.843(4)$[c] | | 0.564 823(130)[c] | 1.667 34(19)[c] |
| $^3\Pi_{0a}$ | $x + 13\,312.69$[d] | $\Delta G_{1/2} \approx 962$[d] | | $B_0 = 0.5701(7)$[d] | $r_0 = 1.6603(10)$[d] |
| $^3\Pi_{0b}$ | $x + 13\,286.43$[d] | $\Delta G_{1/2} \approx 949$[d] | | $B_0 = 0.5697(14)$[d] | $r_0 = 1.6609(20)$[d] |
| $^3\Phi_2$ | $x + 12\,875.23$[d] | $\Delta G_{1/2} \approx 944$[d] | | $B_0 = 0.5691(4)$[d] | $r_0 = 1.6618(6)$[d] |
| $[13.9]^3\Pi_1$ | 13 945.230[c] | 968.297(0.008)[c] | 5.291(0.003)[c] | 0.571 310(210)[c] | 1.657 85(30)[c] |
| $[13.9]^3\Phi_4$ | 13 896.059(0.024)[c] | 954.544(0.046)[c] | 5.408(0.011)[c] | 0.569 517(140)[c] | 1.660 46(20)[c] |
| $[13.5]^3\Phi_3$ | 13 474.699[c] | 951.344[c] | 5.625[c] | 0.567 249(136)[c] | 1.663 77(20)[c] |
| $[12.7]^3\Pi_2$ | 12 734.073(0.024)[c] | 977.818(0.046)[c] | 5.165(0.011)[c] | 0.571 873(624)[c] | 1.657 04(90)[c] |
| $[5.7]^1\Delta_2$ | 5679.13(1.15) | 1068(10) | 6.2(3.9) | $B_0 = 0.5964(4)$ | $r_0 = 1.6206(9)$ |
| $^3\Delta_1$ | $x \approx 2044$[e] | $\Delta G_{1/2} \approx 1032$[d] | | $B_0 = 0.5884$[d] | $r_0 = 1.6343$[d] |
| $[0.9]^3\Delta_2$ | 850.386[c] | 1039.14(0.36)[d] | 4.75(0.16)[d] | $B_0 = 0.587\,106(46)$[c] | $r_0 = 1.635\,40(6)$[c] |
| $[0.1]^3\Delta_3$ | 75.953[c] | 1038.77(0.39)[d] | 4.64(0.13)[d] | 0.587 285[d] | 1.635 15[d] |
| $X\,^1\Sigma^+$ | 0 | 1100.0(1.5) | 5.3(0.3) | $B_0 = 0.607\,354(66)$[c] | $r_0 = 1.607\,90(9)$[c] |

[a]All spectroscopic constants reported from external sources are for the $^{102}Ru^{12}C$ isotopomer.
[b]Numbers in parentheses provide $1\sigma$ error limits of the propagated errors, in $cm^{-1}$. For $B_e$, $B_0$, $r_e$, and $r_0$, errors are in units of the last digit quoted. $T_0$ of the $X\,^1\Sigma^+$ state is constrained to be identically zero, and is without error.
[c]From Ref. 14.
[d]From Refs. 2, 3.
[e]Estimated from spin-orbit calculations. See text.

plays an intense *P*-branch, with a much weaker *R*-branch. This is consistent with the expected branch intensities in an $\Omega' = 1 \rightarrow \Omega'' = 2$ emission and establishes that the state lying at 5679 $cm^{-1}$ has $\Omega = 2$. The only reasonable alternative for the state at 5679 $cm^{-1}$ is the $[\ldots]2\delta^3 12\sigma^1$, $^1\Delta_2$ state. Because this state is isoconfigurational with the $[0.1]\,^3\Delta_3$ and $[0.9]\,^3\Delta_2$ states already observed, it should lie within a few thousand wave numbers of them. In fact, this state was previously predicted to lie at ~5200 $cm^{-1}$ based on spin-orbit interactions between it and the $[0.9]\,^3\Delta_2$ state.[14]

Other relatively low energy configurations that may be expected in RuC are $[\ldots]2\delta^3 6\pi^1$ and $[\ldots]2\delta^2 12\sigma^2$. The $^1\Pi_1$, $^1\Phi_3$, $^3\Phi_{4,3}$, and $^3\Pi_{2,1}$ substates of the $[\ldots]2\delta^3 6\pi^1$ configuration have been previously identified and found to lie in the 12 000–18 000 $cm^{-1}$ range. The remaining $^3\Phi_2$ and $^3\Pi_{0^\pm}$ states surely lie far above the observed state at 5679 $cm^{-1}$, and, in fact, it is the $[\ldots]2\delta^3 12\pi^1$, $^1\Pi$ state which is the upper state of the observed emission system. Therefore, as far as the parentage of the $[5.7]\Omega = 2$ state is concerned, we may exclude the $[\ldots]2\delta^3 6\pi^1$ configuration from further consideration.

Finally, while the $^1\Sigma^+$, $^1\Gamma_4$, and $^3\Sigma^-$ states which arise from the $[\ldots]2\delta^2 12\sigma^2$ configuration remain to be experimentally located, these are unlikely candidates for the 5679 $cm^{-1}$ state. First, none of these states possess an $\Omega'' = 2$ level. Second, emission from the $[\ldots]2\delta^3 12\pi^1$, $^1\Pi$ state to these states requires a two-electron transition for the $^1\Sigma^+$ state, and is forbidden by the $\Delta\Omega$ and $\Delta S$ selection rules for the remaining states. In contrast, fluorescence from the $[\ldots]2\delta^3 6\pi^1$, $^1\Pi$ state is a fully allowed one-electron process for emission to either the $[\ldots]2\delta^4$, $^1\Sigma^+$, or $[\ldots]2\delta^3 12\sigma^1$, $^1\Delta_2$ states. The fact that both emissions are observed with high intensity suggests that all of the states involved are dominated by the single configurations listed here. On this basis the 5679 $cm^{-1}$ state is assigned as the $[5.7]\,^1\Delta_2$ state and is considered to be dominated by the $[\ldots]2\delta^3 12\sigma^1$ configuration.

The resolution of this emission is good enough, and the signal strong enough, to partially resolve the rotational lines in the *P*-branch of the band, as shown in Fig. 3. By fitting the measured line positions to the standard expression

$$\nu = \nu_0 + B'J'(J'+1) - B''J''(J''+1), \tag{3.2}$$

while constraining $B'$ to the previously measured value of $B_0(^1\Pi) = 0.555\,115\ cm^{-1}$,[14] a value of $B_0(^1\Delta) = 0.5964 \pm 0.0004\ cm^{-1}$ is obtained for the rotational constant of the $[5.7]\,^1\Delta_2$ state. Because it is only the *P*-branch for which individual lines are resolved, the fit is sensitive primarily to the difference in rotational constants, $B'$-$B''$. Thus by constraining the value of $B'$ to that measured for $^{102}Ru^{12}C$, our fitted value of $B_0(^1\Delta)$ is most appropriately considered to apply to the $^{102}Ru^{12}C$ isotopomer. Converting this value to a bond length then gives $r_0(^1\Delta) = 1.6226 \pm 0.0005$ Å. This value is very similar to the $r_0$ value previously reported for the isoconfigurational $^3\Delta_2$ state of 1.6354 Å,[14] as expected. The vibrational frequencies of the $[5.7]\,^1\Delta_2$ and $[0.9]\,^3\Delta_2$ states are likewise quite similar, with $\omega_e$ given by 1068 and 1042 $cm^{-1}$, respectively. These facts strongly support the assignment of the 5679 $cm^{-1}$ state as the $[\ldots]2\delta^3 12\sigma^1$, $^1\Delta_2$ state.

### 2. Fluorescence from states of the $[\ldots]2\delta^3 6\pi^1$ configuration

One of the objectives of studying RuC using dispersed fluorescence spectroscopy was to confirm the previous assignment of the $[16.2]\Omega = 3$, $[13.9]\Omega = 1$, $[13.5]\Omega = 3$, and $[12.7]\Omega = 2$ states as the $[16.2]\,^1\Phi$, $[13.9]\,^3\Pi_1$, $[13.5]\,^3\Phi_3$, and $[12.7]\,^3\Pi_2$ states, respectively, deriving from the $[\ldots]2\delta^3 6\pi^1$ configuration.[14] First, dispersed fluorescence from the $[16.2]\,^1\Phi$ state was examined. Emission from this state is observed only to the $[0.9]\,^3\Delta_2$ and $[5.7]\,^1\Delta_2$ states. As argued previously,[14] the $[16.2]\,^1\Phi$ state is in reality a strongly mixed state, with significant $^1\Phi$ and $^3\Phi_3$ character. As a result, the observed emission to both the $[0.9]\,^3\Delta_2$ and $[5.7]\,^1\Delta_2$ states is expected. Fluorescence from the $[13.5]\,^3\Phi_3$ state is observed to the $[0.9]\,^3\Delta_2$ and $[0.1]\,^3\Delta_3$ states. Emission to the $[5.7]\,^1\Delta_2$ state would also be expected, due to the strong mixing of $^1\Phi_3$ character into this upper state wave function, but this emission lies too far to the red to be detected in the present experiments. Fluorescence from the $[13.9]\,^3\Pi_1$ state is observed only to the $[0.9]\,^3\Delta_2$ state, and emission from the $[12.7]\,^3\Pi_2$ state is also observed only to the $[0.1]\,^3\Delta_3$ state. These results satisfy the $\Delta\Sigma = 0$ selection rule, and are again expected.

These emission patterns agree with the predictions previously made by Langenberg *et al.*,[14] and validate the assignments of the upper states. The only surprise is the observation of the $[13.5]\,^3\Phi_3 \rightarrow [0.1]\,^3\Delta_3$ band system in fluorescence. This spin-forbidden, $\Delta\Sigma = 1$, emission process indicates that at least one of the $[13.5]\,^3\Phi_3$ or $[0.1]\,^3\Delta_3$ states is contaminated by spin-orbit mixing with a state having different values of $\Lambda$ and $\Sigma$. If the $^3\Delta_3$ state is mixed with another Hund's case (a) state, contamination by a $^3\Phi_3$ or $^1\Phi$ state would allow the observed emission to occur; if it is the $^3\Phi_3$ state that is mixed with another state, an admixture of a $^3\Delta_3$ state would enable the emission to occur. Of these possibilities, it seems more likely that it is the higher energy $^3\Phi_3$ state that is mixed. A likely source of the contamination is then the $[\ldots]2\delta^3 13\sigma^1$, $^3\Delta_3$ state, which is optically connected to the $[0.1]\,^3\Delta_3$ state by a strongly allowed $13\sigma \rightarrow 12\sigma$ one-electron transition. This $[\ldots]2\delta^3 13\sigma^1$, $^3\Delta_3$ state also has a non-zero spin-orbit matrix element with the $[\ldots]2\delta^3 6\pi^1$, $^3\Phi_3$ state, so that spin-orbit mixing of these states is entirely plausible.

### 3. Comparison to theoretical calculations

The most thorough calculation to date of the low-energy states of RuC has been recently reported by Shim and Gingerich.[46] These investigators have performed a complete active space, self-consistent field (CASSCF) calculation, followed by a multireference configuration interaction (MRCI) calculation. Relativistic and spin-orbit effects were then incorporated using perturbation theory. The calculation was done with a large basis set, and is in superb agreement with our present and previous[14] experiments. The $X\,^1\Sigma^+$ state is

TABLE VI. Dispersed fluorescence excitation and emission bands of PdC.

| Excitation | | | Levels observed in emission | | | | |
|---|---|---|---|---|---|---|---|
| Band system[a] | $\nu_0$[b] | $v'$-$v''$ | $X\,^1\Sigma^+$ | $[2.2]^3\Pi_{0-}$ | $[2.3]^3\Pi_{0+}$ | $[2.5]^3\Pi_1$ | $[2.8]^3\Pi_2$ |
| $[17.9]^3\Sigma_1^+ - X\,^1\Sigma^+$ | 17 867.0328 | 0-0 | | 0 | 0 | 0 | 0 |
| | 18 660.7493 | 1-0 | | 1 | 1 | 1 | 1 |
| $[22.3]\Omega' = 0^+ - X\,^1\Sigma^+$ | 22 253.5301 | 0-0 | 0-5 | | 0-3 | | |
| | 22 685.4603 | 1-0 | 0-2, 4.5 | | 0, 1, 3, 4 | | |
| | 23 152.1891 | 2-0 | 0-3, 5 | | 0, 1 | | |
| | 23 638.7036 | 3-0 | 0-3, 6, 7 | | 0-2, 4, 5 | | |
| | 24 118.7258 | 4-0 | 0, 2, 5 | | 0, 1 | | |
| | 24 577.7072 | 5-0 | 0, 2, 4 | | 0, 1, 3 | | |
| | | 6-0 | 0-4, 6 | | 0-2 | | |
| $[22.1]\Omega' = 0^+ - X\,^1\Sigma^+$ | 23 546.0557 | 3-0 | 0, 1, 3-6 | | 0-2 | | |
| | 24 006.2499 | 4-0 | 0 | | 0 | | |
| | 24 459.0106 | 5-0 | 0 | | 1 | | |
| | 24 904.9719 | 6-0 | 3, 4, 6 | | 0-3 | | |
| $\Omega' = 0^+ - X\,^1\Sigma^+$ | 22 569.3035 | - | 0-2, 4, 5, 7 | | 0-2, 4, 5 | | |
| $\Omega' = 0^+ - X\,^1\Sigma^+$ | 23 351.7513 | - | 0, 2-5 | | 1-4 | | |

[a]Band systems from Ref. 15 are designated as described therein, with the number in square brackets providing the energy of the $v=0$ level, in thousands of $cm^{-1}$.

[b]$\nu_0$ provides the band origin of the excitation band for $^{105}Pd^{12}C$, in $cm^{-1}$ (Ref. 15). The actual excitation wave number employed was adjusted to maximize the fluorescence signal and typically fell within 5 $cm^{-1}$ of $\nu_0$.

calculated to have $r_e = 1.616$ Å and $\omega_e = 1085\,cm^{-1}$, in comparison to experimental values of $r_0 = 1.608$ Å and $\omega_e = 1102\,cm^{-1}$. The $^3\Delta_3$ state is predicted to have $T_0 = 35\,cm^{-1}$, $r_e = 1.632$ Å, and $\omega_e = 1064\,cm^{-1}$, in comparison to experimental values of $T_0 = 76\,cm^{-1}$, $r_e = 1.635$ Å, and $\omega_e = 1039\,cm^{-1}$. The $^3\Delta_2$ state is calculated to have $T_0 = 761\,cm^{-1}$, $r_e = 1.632$ Å, and $\omega_e = 1064\,cm^{-1}$, in comparison with the experimental values of $T_0 = 850\,cm^{-1}$, $r_e = 1.635$ Å, and $\omega_e = 1039\,cm^{-1}$. Finally, calculation of the $^1\Delta_2$ state gives $T_0 = 6204\,cm^{-1}$, $r_e = 1.618$ Å, and $\omega_e = 1086\,cm^{-1}$, which compare to the measured values of $T_0 = 5679\,cm^{-1}$, $r_0 = 1.621$ Å, and $\omega_e = 1068\,cm^{-1}$. This agreement between this calculation and experiment demonstrates that low-lying electronic states of the late $4d$ transition metal carbides can be calculated to uncanny accuracy, provided large basis sets and extensive treatments of electron correlation are employed.

## C. PdC

Dispersed fluorescence spectra were obtained from 15 excitation bands of PdC that were originally observed by Langenberg, Shao, and Morse.[15] Extensive vibrational progressions were observed for two lower states, and emission to $v=0$ and 1 was detected for three other lower states. A list of the bands excited and the resulting emission bands is found in Table V. The vibronic levels identified from this work and the resulting spectroscopic constants are listed in Table VI.

### 1. Fluorescence from $\Omega = 0$ states

Excitation of the $\Omega' = 0 \leftarrow X\Omega'' = 0$ transitions observed previously in this group by R2PI spectroscopy led to the observation of long vibrational progression in emission to two electronic states: the $\Omega = 0$ ground state and a state at 2290 $cm^{-1}$.[15] To determine the $\Omega$ value of the 2290 $cm^{-1}$ state, a comparison of the rotational contours for emission to the ground state and to the 2290 $cm^{-1}$ state was made. The rotational contours resulting from excitation of the $[22.3]\Omega' = 0 \leftarrow X\Omega'' = 0$, 0-0 band are displayed in Fig. 4. For emission to the ground state, the $\Omega = 0 \rightarrow \Omega = 0$ emission is expected to display only $P$- and $R$-branches, consistent with what is observed in the upper panel of Fig. 4. The similar relative branch intensities found for emission to the 2290 $cm^{-1}$ state, along with the absence of a $Q$-branch, identifies the 2290 $cm^{-1}$ state as having $\Omega = 0$ as well. Further, since the upper state of the excitation band is linked to the ground state and the 2290 $cm^{-1}$ state by optical transitions, the three $\Omega = 0$ states must all have the same parity. Either all three have $\Omega = 0^+$ or all three have $\Omega = 0^-$.

The two most likely candidates for the ground configuration of PdC are $[\ldots]12\sigma^2$ and $[\ldots]12\sigma^1 6\pi^1$. The alternative of the $[\ldots]6\pi^2$ ground configuration, supported by early calculations,[42] is excluded by more recent high-level calculations.[40,43,47] The question now is whether the $[\ldots]12\sigma^2$, $^1\Sigma^+$ state is the ground state, or if the high energy of the $5s$ orbital in atomic Pd causes $[\ldots]12\sigma^1 6\pi^1$, $^3\Pi$ to emerge as the ground state. The diagonal matrix elements of the spin-orbit operator split the $^3\Pi$ state into its $\Omega = 0$, 1, and 2 levels, with an expected ordering of $\Omega = 0 < \Omega = 1 < \Omega = 2$. Further off-diagonal spin-orbit interactions, primarily with the nearby $[\ldots]12\sigma^2$, $^1\Sigma^+$ state,[43] then mix the $^3\Pi_{0^+}$ and $^1\Sigma^+$ states, causing a separation between the $^3\Pi_{0^+}$ and $^3\Pi_{0^-}$ levels.

The observation of two low-lying $\Omega = 0$ states reached by fluorescence from an $\Omega = 0$ state strongly suggests that all three $\Omega = 0$ states have $\Omega = 0^+$. The alternative possibility, that all three $\Omega = 0$ states have $\Omega = 0^-$, is unlikely because the low-lying configurations of $[\ldots]12\sigma^2$, $[\ldots]12\sigma^1 6\pi^1$, and $[\ldots]6\pi^2$ only generate one $\Omega = 0^-$ state. On this basis both the ground state and the $[2.3]\Omega = 0$ state are assigned as

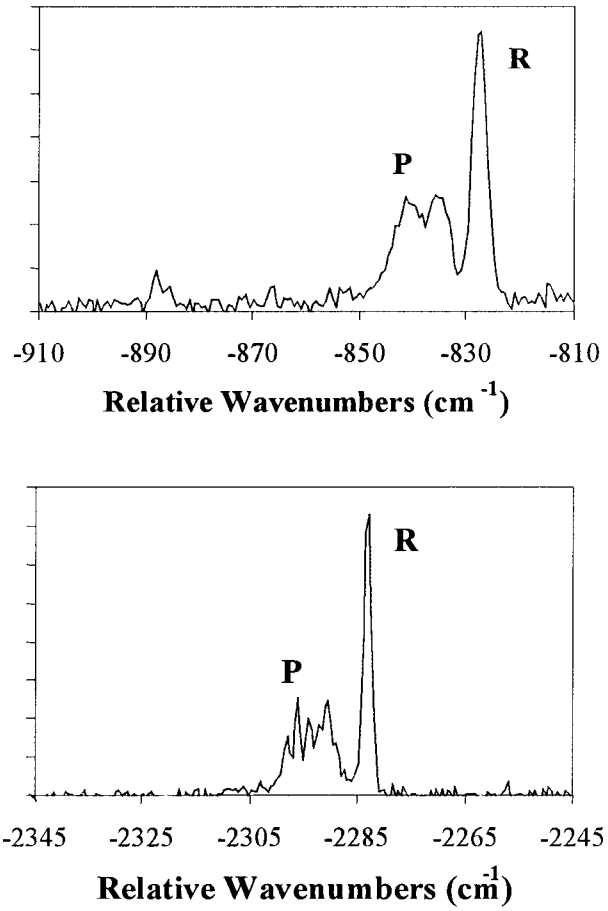


FIG. 4. Rotational band contour obtained by dispersed fluorescence of the 0-1 band of the $[22.3]\Omega'=0^+\rightarrow X\,^1\Sigma^+$ system of PdC (upper panel), compared to the 0-0 band of the $[22.3]\Omega'=0^+\rightarrow[2.3]^3\Pi_{0+}$ system (lower panel).

$\Omega=0^+$. The problem is now reduced to assigning these to the $^1\Sigma^+(\Omega=0^+)$ and $^3\Pi_{0+}$ states.

### 2. Fluorescence from the $[17.9]\Omega=1$ state

Dispersed fluorescence from the $[17.9]\Omega=1$ state exhibited an unusual pattern, as displayed in Fig. 5. Fluorescence from the $v'=0$ level results in a set of four emission bands, and a complementary set of four emission bands is observed in fluorescence from $v'=1$. No other emissions are observed, except for a possible emission to $v''=0$ of the ground state, which is masked by scattered excitation light.

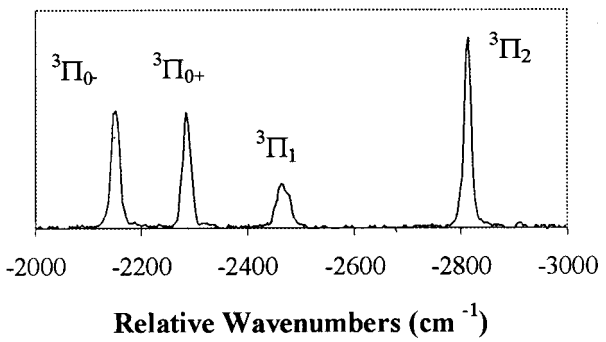


FIG. 5. Dispersed fluorescence of PdC obtained following excitation of the $[17.9]^3\Sigma_1^+\leftarrow X\,^1\Sigma^+$, 0-0 band. Emission to the $\Omega=0^-$, $0^+$, 1, and 2 substates of the $[\ldots]12\sigma^16\pi^1$, $^3\Pi$ state is observed. The $^3\Pi_1$ substate is accessed via collisional deactivation of the $^3\Sigma_1^+$ state to the $^3\Sigma^+(0^-)$ state, which lies 16.5 $cm^{-1}$ lower in energy.

The four emission bands observed in the $v=0$ and $v=1$ excitations are clearly too closely and too erratically spaced to constitute a vibrational progression in a low-lying state. Neither are they atomic emission lines resulting from some sort of multiphoton excitation process involving larger $Pd_n$ clusters or other species, because they require excitation specifically into the $[17.9]\Omega=1$, $v=0$ or $v=1$ levels for their observation, and their absolute wave numbers shift 10–35 $cm^{-1}$ depending on the vibrational level excited. Instead, they appear to be due to four distinct spin-orbit states whose potential curves are so similar to that of the $[17.9]\Omega=1$ state that only $\Delta v=0$ fluorescence has significant Franck–Condon factors. Thus excitation of the $v=0$ level of the $[17.9]\Omega=1$ state leads to fluorescence to the $v=0$ levels of the four states, while excitation of $v=1$ leads to fluorescence to $v=1$. From this it may be concluded that the four states have $T_0=2157$, 2289, 2470, and 2818 $cm^{-1}$ and $\Delta G_{1/2}=765$, 782, 762, and 760 $cm^{-1}$, respectively.

The similarity between these $\Delta G_{1/2}$ values and the strong propensity for $\Delta v=0$ emission shared by the four states together suggest that the four states are the spin-orbit substrates of a common $\Lambda$-$S$ term. Based on theoretical calculations of a low-lying $[\ldots]12\sigma^16\pi^1$, $^3\Pi$ term, it seems likely that these are the $\Omega=0^-$, $0^+$, 1, and 2 substrates of the predicted $^3\Pi$ term. In this context, we note that the vibrational frequency of the $^3\Pi$ term has been calculated to be $\omega_e=794\,cm^{-1}$ by Russo *et al.*[40] and 762 $cm^{-1}$ by Tan *et al.*,[43] in close agreement with the $\Delta G_{1/2}$ values listed above. Russo *et al.* also predict the $^3\Pi$ term to lie 2718 $cm^{-1}$ above the ground $^1\Sigma^+$ state, in good agreement with the spin-orbit averaged value of $T_0=2504\,cm^{-1}$.[40] On this basis, the assignment of the levels as arising from the $[\ldots]12\sigma^16\pi^1$, $^3\Pi$ term seems secure. It should also be noted that the calculated bond lengths of the $^3\Pi$ term (1.741 Å[40] and 1.721 Å[43]) are similar to the bond length measured for the $[17.9]\Omega=1$ state, $r_e=1.709$ Å.[15] Allowing for the fact that *ab initio* calculations tend to overestimate bond lengths, this nicely explains the strong $\Delta v=0$ Franck–Condon restriction on the fluorescence patterns.

Next, we must assign $\Omega$ quantum numbers to the observed states. According to Hund's rule, a $[\ldots]12\sigma^16\pi^1$, $^3\Pi$ term should be regular, with the $\Omega$ levels falling in the order $0^+$, $0^-<1<2$. The ordering of the $\Omega=0^+$, $0^-$ pair cannot be deduced from the electronic configuration. This splitting results from off-diagonal spin-orbit couplings to other states, and is therefore dependent on the electronic character and relative energy of the other states. Tan *et al.* have noted that a significant spin-orbit interaction exists between the $[\ldots]12\sigma^2$, $^1\Sigma^+$ state and the $[\ldots]12\sigma^16\pi^1$, $^3\Pi_{0+}$ substate.[43] Having located the $^3\Pi$ levels, we may now deduce that the $[\ldots]12\sigma^2$, $^1\Sigma^+$ state is indeed the ground state of PdC. This implies that the $^3\Pi_{0+}$ level undergoes a significant spin-orbit perturbation *from below*. Thus the expected energy ordering of the $^3\Pi_\Omega$ levels is $0^-<0^+\ll1\ll2$, and the substates with $T_0=2157$, 2289, 2470, and 2818 $cm^{-1}$ may

be assigned as $[\ldots]12\sigma^1 6\pi^1$, $^3\Pi_{0^-}$, $^3\Pi_{0^+}$, $^3\Pi_1$, and $^3\Pi_2$, respectively.

It should be noted that the $^3\Pi_{0^-}$, $^3\Pi_1$, and $^3\Pi_2$ spin-orbit components have very similar $\Delta G_{1/2}$ values of 765, 762, and 760 $cm^{-1}$, respectively, while the $\Delta G_{1/2}$ value of the state assigned as $^3\Pi_{0^+}$ is 782 $cm^{-1}$. Without a doubt this is the result of spin-orbit mixing with the $[\ldots]12\sigma^2$, $^1\Sigma^+$ ground state, which has an even higher value of $\Delta G_{1/2} = 834\,cm^{-1}$. In addition, the low-lying $\Omega=0$ state discussed in the previous subsection lies at the same energy and has the same value of $\Delta G_{1/2}$ as this $^3\Pi_{0^+}$ state; therefore, these two states are one and the same. The existence of many upper states which can fluoresce to both the $[\ldots]12\sigma^2$, $^1\Sigma^+$ ground state and the $[\ldots]12\sigma^1 6\pi^1$, $^3\Pi_{0^+}$ state, but not to the other $^3\Pi_\Omega$ levels, suggests strongly that the $^3\Pi_{0^+}$ state borrows much of its intensity in these emissions from the $[\ldots]12\sigma^2$, $^1\Sigma^+$ ground term.

### 3. Assignment of the $[17.9]\Omega=1$ state

With the lower state assignments in place, we are now able to consider the $\Lambda$-$S$ term from which the $[17.9]\Omega=1$ state derives. In the initial R2PI spectroscopic study,[15] this state was found to display significant hyperfine splitting in the $^{105}Pd^{12}C$ isotopic modification. In fact, the hyperfine splitting was so large that it could only arise from a Fermi contact interaction involving an unpaired electron in a $\sigma$ orbital with substantial $5s$ character on palladium. This also implied that the $[17.9]\Omega=1$ state is primarily triplet (or higher spin multiplicity) in character. With this fact in mind, it is likely that the oscillator strength for the $[17.9]\Omega=1 \leftarrow X\,^1\Sigma^+$ absorption derives from the spin-orbit induced admixture of $[\ldots]12\sigma^1 6\pi^1$, $^3\Pi_{0^+}$ character into the ground state wave function. This view is supported by the fact that the only observed fluorescence from the $[17.9]\Omega=1$ state is to the $[\ldots]12\sigma^1 6\pi^1$, $^3\Pi$, $\Omega=0^-$, $0^+$, 1, and 2 substates, and not to the $X\,^1\Sigma^+$ ground state.

The observed fluorescence from the $[17.9]\Omega=1$ state to all four spin-orbit components of the $[\ldots]12\sigma^1 6\pi^1$, $^3\Pi$ state may be used to determine the $\Lambda$-$S$ parentage of the $[17.9]\Omega=1$ state. The $\Omega=0^+$ component of the $[\ldots]12\sigma^1 6\pi^1$, $^3\Pi$ state is known to be contaminated with $[\ldots]12\sigma^2$, $^1\Sigma^+$ character. Likewise, the isoconfigurational spin-orbit interaction between the $[\ldots]12\sigma^1 6\pi^1$, $^3\Pi_1$ and $^1\Pi_1$ states contaminates the state we designate as $^3\Pi_1$ with some $^1\Pi_1$ character. The remaining $\Omega=0^-$ and 2 substates are expected to be fairly pure in $\Lambda$-$S$ character, however, since no states with $\Omega=0^-$ or 2 are calculated to lie within 12 000 $cm^{-1}$ of the $^3\Pi$ states.[43] The observation of strong emissions from the $[17.9]\Omega=1$ state to the $^3\Pi_{0^-}$ and $^3\Pi_2$ substates then strongly suggests that the $[17.9]\Omega=1$ state is dominated by $^3\Sigma$ character. This statement is based on the fact that the only pure $\Omega=1$, $\Lambda$-$S$ state that can fluoresce to both $^3\Pi_{0^-}$ and $^3\Pi_2$ and obey the selection rules $\Delta S=0$ and $\Delta\Sigma=0$ is a $^3\Sigma_1$ state. Fluorescence to $^3\Pi_{0^+}$ also obeys these selection rules, but fluorescence to $^3\Pi_1$ corresponds to a forbidden, $\Delta\Sigma=1$ emission process. Its observation in the dispersed fluorescence spectrum can only be explained by perturbation of the $^3\Sigma_1$ upper state by another state or substate, or by collisional transfer of $^3\Sigma_1$ population to the $^3\Sigma_0$ substate that is expected to lie close in energy.

The large hyperfine splitting in the $[17.9]\Omega=1$ state, which requires an unpaired electron in a $\sigma$ orbital for its explanation, in turn implies that the electronic configuration of the $^3\Sigma$ state must be $[\ldots]12\sigma^1 13\sigma^1$. This further identifies the parity of the $^3\Sigma$ state as $^3\Sigma^+$, and restricts the $\Omega$ values of this state to $\Omega=0^-$ and 1. In $^3\Sigma^-$ states deriving from $\pi^2$ or $\delta^2$ configurations the analogous $\Omega=0^+$ and 1 substates may be separated by tens or even hundreds of wave numbers due to off-diagonal spin-orbit interactions between the $\Omega=0^+$ component and the $^1\Sigma^+$ state that derives from the same $\pi^2$ or $\delta^2$ configuration. In contrast, the splitting of a $^3\Sigma^+$ state into its $\Omega$ substates is typically much smaller, due to the lack of any isoconfigurational spin-orbit couplings. As a result, $^3\Sigma^-$ terms often follow a Hund's case (a) coupling scheme, while this is rarely observed in $^3\Sigma^+$ terms.

We note in this case that the $^3\Sigma_1^+ \leftarrow X\,^1\Sigma^+$ excitation was observed to be perturbed by the $^3\Sigma^+$, $\Omega'=0^-$ component in the R2PI spectroscopy study,[15] and this substate was determined to be located only $2\lambda' = 16.5\pm0.9\,cm^{-1}$ below the $\Omega=1$ component. While a $^3\Sigma_1^+ \rightarrow {}^3\Pi_1$ emission is forbidden, emission from the $^3\Sigma_{0^-}^+$ substrate is allowed. Given the small splitting between these substates, collisional deactivation of the initially excited $^3\Sigma_1^-$ state to the $^3\Sigma_{0^-}^+$ substate could lead to the observed fluorescence to the $^3\Pi_1$ substate. To test this hypothesis, dispersed fluorescence to the $^3\Pi$ state was observed as the molecular beam was excited at points progressively farther downstream from the exit orifice. A related experiment observed the emission as the backing pressure behind the solenoid valve was reduced to near 0 psig. The resulting effect in either case was to observe the molecular beam at points in the expansion where collisions become progressively fewer. If fluorescence to the $^3\Pi_1$ substate were indeed occurring via collisional deactivation of $^3\Sigma_1^+$ to $^3\Sigma_{0^-}^+$ the intensity of emission to $^3\Pi_1$ should decrease relative to the intensity of emission to the other $^3\Pi_\Omega$ components as the collision rate is reduced. This was found to occur, confirming both the findings of the R2PI spectroscopy study and the assignment of the $^3\Pi_1$ state. As a result, the $T_0$ value for the $[2.5]^3\Pi_1$ state is reported as 2453.1 $cm^{-1}$, a value which is reduced from the measured value by the $2\lambda$ value of the $[17.9]\,^3\Sigma^+$ state, to account for the fact that emission to the $^3\Pi_1$ substate originates from the $\Omega'=0^-$ component of the $[17.9]\,^3\Sigma^+$ state. See Table VII for other values.

## IV. DISCUSSION

### A. Spin-orbit interactions and electronic structure

By studying spin-orbit interactions in molecules such as MoC, RuC, and PdC, much can be learned about the electronic structure of the molecule. In this investigation of the low-lying electronic states of the transition metal carbides, we have used the measured spin-orbit splittings to estimate three types of quantities: the energies of states not yet observed, the amount of spin-orbit mixing that occurs between coupled Hund's case (a) states, and the metal and carbon atomic orbital contributions to the various molecular orbitals.

TABLE VII. Vibronic levels of PdC and fitted spectroscopic constants.

| Electronic state | $v$ | Energy ($cm^{-1}$)[a] | Fitted energy ($cm^{-1}$) | Residual ($cm^{-1}$) |
|---|---|---|---|---|
| $X\,^1\Sigma^+$ | 0 | 0 | 0.0 | 0.0 |
| | 1 | 833.6(2.2) | 835.0 | −1.4 |
| | 2 | 1654.1(7.4) | 1657.5 | −3.4 |
| | 3 | 2468.4(3.2) | 2467.4 | 1.0 |
| | 4 | 3264.3(8.6) | 3264.7 | −0.4 |
| | 5 | 4051.8(6.8) | 4049.4 | 2.4 |
| | 6 | 4828.1(7.2) | 4821.6 | 6.5 |
| | 7 | 5580.2(2.8) | 5581.2 | −1.0 |
| $[2.3]^3\Pi_{0+}$ | 0 | 2289.2(4.0) | 2289.1 | 0.1 |
| | 1 | 3071.0(6.2) | 3070.8 | 0.2 |
| | 2 | 3845.9(7.1) | 3845.8 | 0.1 |
| | 3 | 4610.8(5.9) | 4614.1 | −3.3 |
| | 4 | 5378.9(4.9) | 5375.6 | 3.3 |
| | 5 | 6128.3(6.5) | 6130.5 | −2.2 |

| | Fitted spectroscopic constants | | |
|---|---|---|---|
| State | $T_0$ ($cm^{-1}$)[b] | $\omega_e$ ($cm^{-1}$)[b] | $\omega_e x_e$ ($cm^{-1}$)[b] |
| $[2.8]^3\Pi_2$ | 2818.0(2.6) | $\Delta G_{1/2}$=759.9(3.7) | |
| $[2.5]^3\Pi_1$ | 2453.1(2.7) | $\Delta G_{1/2}$=762.3(3.8) | |
| $[2.3]^3\Pi_{0+}$ | 2289.1(3.8) | 788.4(5.4) | 3.4(0.9) |
| $[2.2]^3\Pi_{0-}$ | 2157.1(2.6) | $\Delta G_{1/2}$=765.1(3.7) | |
| $X\,^1\Sigma^+$ | 0 | 847.6(1.6) | 6.3(0.2) |

[a]Numbers in parentheses provide $1\sigma$ error estimates of the averaged data, in $cm^{-1}$.
[b]Numbers in parentheses provide $1\sigma$ error limits of the propagated errors, in $cm^{-1}$. $T_0$ of the $X\,^1\Sigma^+$ state is constrained to be identically zero, and is without error.

The spin-orbit analysis presented here follows procedures analogous to those used in previous studies of NbO[53] and $V_2$, VNb, and $Nb_2$,[54] and is exact within the framework of a two-state model.

### 1. MoC

From the dispersed fluorescence studies of MoC, the $^3\Delta_2$ and $^1\Delta_2$ states deriving from the $[\ldots]2\delta^1 12\sigma^1$ configuration are known to lie at $T_0=4002.5$ and 7834.2 $cm^{-1}$, respectively. If one makes the very reasonable assumption that the $2\delta$ orbitals of MoC are composed purely of $4d\,\delta$ orbitals on Mo, then it is a straightforward process to set up the Hamiltonian matrix for the spin-orbit interactions within the $[\ldots]2\delta^1 12\sigma^1$ configuration. The nonzero matrix elements of the $4\times 4$ Hamiltonian matrix are given in terms of the term energies of the $^3\Delta$ and $^1\Delta$ states, $T_3$ and $T_1$, and the molecular spin-orbit parameter, $a_\delta$, as $\langle {}^3\Delta_3|H|{}^3\Delta_3\rangle = T_3 + a_\delta$, $\langle {}^3\Delta_2|H|{}^3\Delta_2\rangle = T_3$, $\langle {}^3\Delta_1|H|{}^3\Delta_1\rangle = T_3 - a_\delta$, $\langle {}^1\Delta_2|H|{}^1\Delta_2\rangle = T_1$, and $\langle {}^3\Delta_2|H|{}^1\Delta_2\rangle = -a_\delta$. Because the $2\delta$ orbital is assumed to be of pure $4d$ character on Mo, the atomic spin orbit parameter, $\zeta = 595.4\,cm^{-1}$, obtained from a numerical Hartree–Fock calculation on the $4d^5 5s^1$, $^7S$ ground state,[55] provides a reasonable estimate of $a_\delta$. The spin-orbit parameter, $\zeta$, varies significantly with atomic orbital occupation, and the $4d^5 5s^1$ atomic configuration is chosen because it closely mimics the $[\ldots]2\delta^1 12\sigma^1$ configuration of the MoC molecule. In each case one electron is either in the $5s$ atomic orbital or in a molecular orbital that is primarily $5s$ in character (the $12\sigma$ orbital).

Using the measured energies of the $^3\Delta_2$ and $^1\Delta_2$ levels of 4002.5 and 7834.2 $cm^{-1}$, along with the estimate of $a_\delta = 595.4\,cm^{-1}$, the energies of the unobserved $^3\Delta_1$ and $^3\Delta_3$ levels are predicted as 3502 and 4693 $cm^{-1}$, respectively. These energies are in good agreement with measurements of the photoelectron spectrum of $MoC^-$, which place the $^3\Delta_1$ and $^3\Delta_3$ levels at $3549\pm 160\,cm^{-1}$ and $4759\pm 240\,cm^{-1}$, respectively.[17]

Because of the off-diagonal spin-orbit matrix element that couples the $[\ldots]2\delta^1 12\sigma^1$, $^3\Delta_2$ and $^1\Delta_2$ states, the molecular states take on mixed singlet–triplet character. The extent of mixing may be determined by diagonalizing the Hamiltonian matrix and obtaining the resulting eigenfunctions. For a general two-state problem this gives the upper and lower energy eigenfunctions, $\Psi_+$ and $\Psi_-$, in terms of the basis functions $\phi_1$ and $\phi_2$, as

$$\Psi_+ = c_1\phi_1 + c_2\phi_2, \tag{4.1}$$

$$\Psi_- = -c_2\phi_1 + c_1\phi_2, \tag{4.2}$$

with

$$|c_1|^2 = \frac{2x^2}{1-\sqrt{1+4x^2}+4x^2}, \tag{4.3}$$

where $x = H_{12}/(H_{11}-H_{22})$. The value of $|c_1|^2$ gives the fractional contribution of $\phi_1$ to the overall wave function; $|c_2|^2$ is then given simply as $1-|c_1|^2$. In this manner, the state designated as $[4.0]\,^3\Delta_2$ is found to be a mixture of 97.5% $^3\Delta_2$ and 2.5% $^1\Delta_2$. Similarly, the state designated as $[7.8]\,^1\Delta_2$ consists of 97.5% $^1\Delta_2$ and 2.5% $^3\Delta_2$ character.

### 2. RuC

The spin-orbit interactions among the states of the $[\ldots]2\delta^3 12\sigma^1$ configuration of RuC are nearly identical to those among the states of the $[\ldots]2\delta^1 12\sigma^1$ configuration of MoC. The only significant difference is that the $[\ldots]2\delta^3 12\sigma^1$ configuration of RuC leads to an inverted spin-orbit structure in the $^3\Delta$ state. For RuC, however, the energies of the $^3\Delta_3$, $^3\Delta_2$, and $^1\Delta_2$ states are experimentally known, allowing us to determine the molecular spin-orbit parameter, $a_\delta$, directly from the data as $a_\delta = 984\,\mathrm{cm}^{-1}$. This solution predicts the energy of the $^3\Delta_1$ level as 2044 $\mathrm{cm}^{-1}$. Surprisingly, a second solution also exists, giving $a_\delta = 2205\,\mathrm{cm}^{-1}$ and predicting the $^3\Delta_1$ level at 4485 $\mathrm{cm}^{-1}$. Calculations using the numerical Hartree–Fock program of Charlotte Froese–Fischer,[55] however, predict the atomic spin-orbit parameter $\zeta_{4d}$(Ru) as 855, 943, and 1041 $\mathrm{cm}^{-1}$ for the $[\ldots]4d^8$, $^3F$; $[\ldots]4d^7 5s^1$, $^5F$; and $[\ldots]4d^6 5s^2$, $^5D$ states of neutral atomic Ru, respectively. These values compare well to the first root of this problem ($a_\delta = 984\,\mathrm{cm}^{-1}$), and differ greatly from the second root ($a_\delta = 2205\,\mathrm{cm}^{-1}$). On this basis the first root is selected, and the energy of the $^3\Delta_1$ level is predicted as 2044 $\mathrm{cm}^{-1}$. As this prediction uses a known value for $E(^1\Delta_2)$ in its derivation, it may be considered an improvement over the earlier estimate of ~2150 $\mathrm{cm}^{-1}$ given in our previous study of RuC.[14] It is also gratifying that the value of $a_\delta = 984\,\mathrm{cm}^{-1}$ obtained for these states lies closest to the value calculated for the $[\ldots]4d^7 5s^1$, $^5F$ atomic term [$\zeta_{4d}(\mathrm{Ru}) = 943\,\mathrm{cm}^{-1}$]. Given that the $12\sigma$ orbital in this molecule has roughly 83% $5s_{\mathrm{Ru}}$ character,[14] it makes sense that the atomic $\zeta$ parameter calculated for a $4d^7 5s^1$ atomic configuration should provide a good estimate of the $a_\delta$ parameter in the $[\ldots]2\delta^3 12\sigma^1$ states of the molecule.

Like the $2\delta^1 12\sigma^1$, $^3\Delta_2$ and $^1\Delta_2$ states of MoC, the $2\delta^3 12\sigma^1$, $^3\Delta_2$ and $^1\Delta_2$ states of RuC are mixed by spin-orbit interactions. Using the procedure outlined above, the state identified as [0.9] $^3\Delta_2$ is calculated to have approximately 96% $^3\Delta_2$ character and 4% $^1\Delta_2$ character. Likewise, the state designated as [5.7] $^1\Delta_2$ is calculated to have 96% $^1\Delta_2$ and 4% $^3\Delta_2$ character.

### 3. PdC

There are two important spin-orbit interactions to consider in PdC. The first is the isoconfigurational spin-orbit interaction between the $[\ldots]12\sigma^1 6\pi^1$, $^3\Pi_1$ and $^1\Pi_1$ states, while the second is the observed spin-orbit coupling between the $[\ldots]12\sigma^1 6\pi^1$, $^3\Pi_{0^+}$ state and the $[\ldots]12\sigma^2$, $^1\Sigma^+(\Omega = 0^+)$ state. The former is similar to the spin-orbit interactions between the $[\ldots]2\delta^1 12\sigma^1$, $^3\Delta_1$ and $^1\Delta_1$ states of MoC previously discussed. In this case, however, the off-diagonal matrix element coupling these states is given by $-1/2a_\pi$, where $a_\pi$ is no longer given simply by the atomic $\zeta_{4d}$(Pd) parameter because of orbital mixing between the $4d\pi_{\mathrm{Pd}}$ and $2p\pi_{\mathrm{C}}$ atomic orbitals.[56] As discussed above, the $\Omega = 2$ and $0^-$ components of the $^3\Pi$ state are considered to be unperturbed, and the difference between them provides $a_\pi = 660.9\,\mathrm{cm}^{-1}$. The displacement of the $^3\Pi_1$ level from the average of the $^3\Pi_2$ and $^3\Pi_{0^-}$ energies is then due primarily to the off-diagonal spin-orbit interaction between $^3\Pi_1$ and the isoconfigurational $^1\Pi_1$ state. This may be used to calculate the energy of the $^1\Pi$ state, which is predicted to lie 5657 $\mathrm{cm}^{-1}$ above the ground state, or 3204 $\mathrm{cm}^{-1}$ above the $^3\Pi_1$ state. This latter result compares reasonably well with the exchange splitting in Pd between the $4d^9 5s^1$, $^3D_2$ and $^1D_2$ states of 3966.8 $\mathrm{cm}^{-1}$,[57] and with the $^3\Pi_1 - {}^1\Pi_1$ splitting calculated by *ab initio* methods to be 4800 $\mathrm{cm}^{-1}$.[43] Following the procedure established above, we conclude that the state designated as [2.5] $^3\Pi_1$ state has 99% $^3\Pi_1$ character and 1% $^1\Pi$ character. Likewise, the $^1\Pi$ state predicted to lie at 5657 $\mathrm{cm}^{-1}$ is contaminated with about 1% $^3\Pi_1$ character. It should be emphasized that the calculated position of the unobserved $^1\Pi$ state is quite sensitive to the measured energy of the $^3\Pi_1$ state, since a 1 $\mathrm{cm}^{-1}$ change in this energy leads to a 94 $\mathrm{cm}^{-1}$ change in the predicted energy of the $^1\Pi$ state. Allowing for this error, we estimate that our predicted $^1\Pi$ energy is probably correct to within about 500 $\mathrm{cm}^{-1}$.

In considering the second-order spin-orbit interaction between the $X\,^1\Sigma^+$ and [2.3] $^3\Pi_{0^+}$ states, the contribution of the off-diagonal spin-orbit element may be determined by observing the separation between the $^3\Pi_{0^-}$ component, which is assumed to be unperturbed, and the $^3\Pi_{0^+}$ component. From the measured $^3\Pi_{0^+} - {}^3\Pi_{0^-}$ splitting, an off-diagonal spin-orbit matrix element of 533.6 $\mathrm{cm}^{-1}$ may be deduced. This figure is quite large in comparison to the separation between the $X\,^1\Sigma^+$ and [2.3] $^3\Pi_{0^+}$ states, leading to significant mixing of the $^1\Sigma^+$ and $^3\Pi_{0^+}$ wave functions. The ground state, designated as $X\,^1\Sigma^+$, is calculated to have approximately 94% $^1\Sigma^+$ character and 6% $^3\Pi_{0^+}$ character. Similarly, the state designated as [2.3] $^3\Pi_{0^+}$ has 94% $^3\Pi_{0^+}$ character and 6% $^1\Sigma^+$ character.

With the measured value of $a_\pi = 660.9\,\mathrm{cm}^{-1}$, the contributions of the $4d\pi_{\mathrm{Pd}}$ and $2p\pi_{\mathrm{C}}$ atomic orbitals to the $6\pi$ molecular orbital may be estimated under the assumptions (1) that no other atomic orbitals contribute, and (2) that the $^3\Pi$ state is well-described by a $[\ldots]12\sigma^1 6\pi^1$ single configurational wave function. With these assumptions, the molecular spin-orbit parameter, $a_\pi$, is given as

$$a_\pi = \langle 6\pi|\hat{a}|6\pi\rangle = |c_1|^2 \zeta_{4d}(\mathrm{Pd}) + |c_2|^2 \zeta_{2p}(\mathrm{C}), \tag{4.4}$$

where the $6\pi$ molecular orbital is written as

$$|6\pi\rangle = c_1|4d\pi_{\mathrm{Pd}}\rangle + c_2|2p\pi_{\mathrm{C}}\rangle. \tag{4.5}$$

To calculate the values of $|c_1|^2$ and $|c_2|^2$, we employ estimates of the atomic spin-orbit parameters $\zeta_{4d}(\mathrm{Pd}) = 1389\,\mathrm{cm}^{-1}$ and $\zeta_{2p}(\mathrm{C}) = 32\,\mathrm{cm}^{-1}$, which are obtained for the $4d^9 5s^1$, $^3D$ term of Pd and either the $2s^2 2p^2$, $^3P$ or $2s^1 2p^3$, $^5S^0$ term of C by numerical Hartree–Fock calculations using the program written by Charlotte Froese–Fischer.[55] If we assume the overlap of the $4d\pi_{\mathrm{Pd}}$ and $2p\pi_{\mathrm{C}}$ atomic orbitals is negligible, then the contributions of the Pd and C orbitals are 46% and 54%, respectively. When an overlap integral of $S = 0.12$ is assumed, the contribution of the $2p\pi_{\mathrm{C}}$ orbital increases to 68%, but the Pd atomic orbital contribution remains 46%. The remainder is the overlap population, defined as $2c_1c_2S$, where $S$ is the $\langle 4d\pi_{\mathrm{Pd}}|2p\pi_{\mathrm{C}}\rangle$ overlap integral, and is numerically equal to −13%.

The small variation in $|c_1|^2$ with the value of the overlap integral, $S$, is a simple result of the fact that the molecular spin-orbit parameter, $a_\pi$, depends almost entirely on $|c_1|^2$, rather than $|c_2|^2$, because of the large value of $\zeta_{4d}$(Pd) relative to $\zeta_{2p}$(C). Because $\zeta_{2p}$(C) is so small, the coefficient of the $2p\pi_C$ orbital can vary significantly without greatly influencing the value of $a_\pi$. Conversely, the $\zeta_{4d}$ parameter for Pd is so large that the coefficient of the $4d\pi_{Pd}$ orbital cannot vary widely without causing the value of $a_\pi$ to change. As a result, the $6\pi$ orbital is rather accurately determined to contain about 46% $4d\pi_{Pd}$ character. This is a bit higher than the calculated result of 35% Pd character in the $6\pi$ orbital, obtained in a local spin density calculation by Russo *et al.*[40]

Similarly, the measured spin-orbit interaction between the $X\,^1\Sigma^+$ and $^3\Pi_{0+}$ states may be used to estimate the composition of the $12\sigma$ orbital. Assuming that these states are well-described by the single configurations $[\ldots]12\sigma^2$, $^1\Sigma^+$ and $[\ldots]12\sigma^1 6\pi^1$, $^3\Pi_{0+}$, writing the $6\pi$ orbital as in Eq. (4.5) and the $12\sigma$ orbital as

$$|12\sigma\rangle = b_1|4d\sigma_{Pd}\rangle + b_2|2p\sigma_C\rangle + b_3|5s\sigma_{Pd}\rangle, \tag{4.6}$$

and employing the methods described by Lefebvre-Brion and Field,[56] the spin-orbit matrix element may be evaluated as

$$\langle X\,^1\Sigma^+|\hat{H}^{SO}|^3\Pi_{0^+}\rangle = \frac{1}{\sqrt{2}}\langle 12\sigma|\hat{a}\hat{l}^-|6\pi_{+1}\rangle$$

$$= \sqrt{3}b_1c_1\zeta_{4d}(Pd) + b_2c_2\zeta_{2p}(C). \tag{4.7}$$

Here $\zeta_{4d}$(Pd) and $\zeta_{2p}$(C) are the spin-orbit parameters for the respective Pd and C atomic orbitals. As in the calculation of $a_\pi$, they are taken to be 1389 and 32 $cm^{-1}$, respectively. From the analysis of the spin-orbit interactions in the $[\ldots]12\sigma^1 6\pi^1$, $^3\Pi$ states, $|c_1|^2$ was determined to be 0.46, giving $c_1 = 0.68$. Likewise, $|c_2|^2$ was thought to fall in the approximate range of 0.54 to 0.68, giving $c_2 = -0.73$ to $-0.83$. Having already determined that $\langle X\,^1\Sigma^+|\hat{H}^{SO}|^3\Pi_{0+}\rangle = 533.6\,cm^{-1}$, and choosing the value $c_2 = -0.78$, Eq. (4.7) then gives

$$1636b_1 - 25b_2 = 533.6. \tag{4.8}$$

While this single equation in two variables cannot be solved, it nevertheless places stringent limits on the amount of $4d\sigma_{Pd}$ character in the $12\sigma$ orbital. This results from the large factor that multiplies $b_1$ and the much smaller factor that multiplies $b_2$. Even for values of $b_2$ covering the extreme range from $-1$ to 1, $b_1$ only ranges between 0.311 and 0.341, giving $|b_1|^2$ in the range of 0.097 to 0.12. Thus it is fair to say that the $12\sigma$ orbital of PdC has approximately 10–12% $4d\sigma_{Pd}$ character. In the related molecule, RuC, hyperfine interactions have been measured for the $^{101}Ru^{12}C$ isotopomer, and the magnitude of the hyperfine splitting has shown the $12\sigma$ orbital to be roughly 83% $5s_{Ru}$ in character.[14] Thus the small amount of $4d\sigma$ character (10%–12%) found for this orbital in the case of PdC is not surprising. In fact, it is in stunning agreement with the results of a local spin density calculation on PdC by Russo *et al.*, who obtain 9% $4d\sigma$ character in the $12\sigma$ orbital in the $[\ldots]12\sigma^1 6\pi^1$, $^3\Pi$ state and 12% $4d\sigma$ character for this orbital in the $[\ldots]12\sigma^2$, $^1\Sigma^+$ ground state.[40]

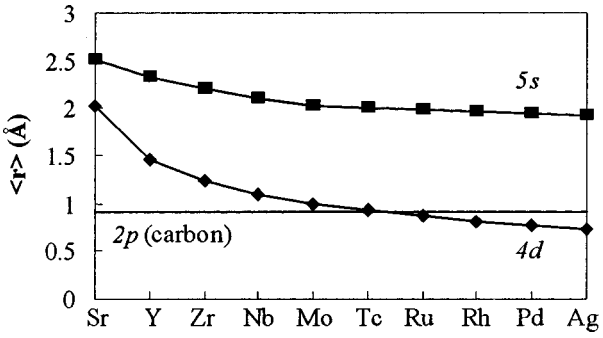


FIG. 6. Numerical Hartree–Fock calculations of the orbital radial expectation value $\langle r\rangle$ for the $4d$ and $5s$ orbitals of the $4d$ transition metal atoms in their $4d^n5s^1$ configurations. For comparison, the radial expectation value for the $2p$ orbitals of carbon, $\langle r\rangle_{2p}$, is indicated by the horizontal line.

Perhaps the most surprising aspect of this result is that such a small amount of $4d_\sigma$(Pd) character (10%–12%) could result in such a large off-diagonal spin-orbit matrix element (533.6 $cm^{-1}$). Several factors contribute to this effect. First, evaluation of the $\hat{l}^-$ operator in Eq. (4.7) leads to a numerical factor of $\sqrt{6}$ in the result, thereby magnifying the spin-orbit matrix element substantially. Second, the spin-orbit matrix element depends on $b_1$ while the amount of $4d_\sigma$ character depends on $|b_1|^2$. Thus for example, a reduction in the amount of $4d_\sigma$ character in the $12\sigma$ orbital by a factor of 4 only reduces the spin-orbit matrix element by a factor of 2. Even if the $12\sigma$ orbital had only 3% $4d_\sigma$(Pd) character, the resulting spin-orbit matrix element would still be approximately 265 $cm^{-1}$. Finally, the large magnitude of $\zeta_{4d}$(Pd) is ultimately responsible for the size of this coupling matrix element.

### B. Chemical bonding trends in the 4*d* transition metal carbides

An important factor in determining the strength of the covalent bond is the extent to which the atomic orbitals on neighboring atoms can overlap. Optimal orbital overlap occurs when the atomic orbitals on the two centers are of comparable size, provided there are no other constraints that prevent the atoms from approaching one another closely enough to achieve this overlap. As illustrated in Fig. 6, the $4d$ orbitals contract monotonically as one traverses the $4d$ series, from $\langle r\rangle_{4d} = 1.456$ Å for the $4d^2 5s^1$, $^4F$ term of yttrium to $\langle r\rangle_{4d} = 0.765$ Å for the $4d^9 5s^1$, $^3D$ term of palladium.[55] These values compare to a mean orbital radius for the $2p$ orbitals of carbon of $\langle r\rangle_{2p} = 0.91$ Å.[55] Thus this series of molecules provides an opportunity to investigate the effects of $4d$ orbital size on the chemical bonding in a series of related transition metal carbides. Particularly noteworthy in this regard are the molecules NbC, MoC, and RuC, which differ in their ground electronic states only by the number of nonbonding $2\delta$ electrons that are present. The presence or absence of a $2\delta$ electron should have little effect on the chemical bonding with carbon, so the bonding in this set of molecules differs primarily because of the variation in the size of the $4d$ orbitals from metal to metal.

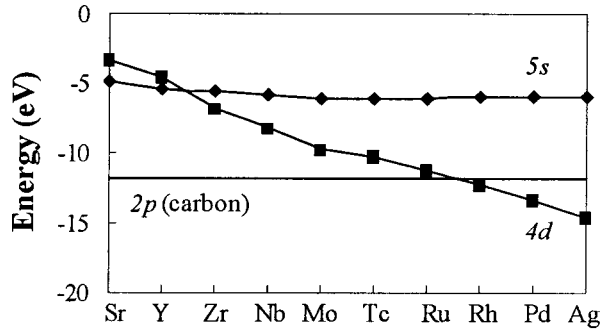


FIG. 7. Numerical Hartree–Fock calculations of the orbital energies of the $4d$ and $5s$ orbitals of the $4d$ transition metal atoms in their $4d^n5s^1$ configurations. For comparison, the orbital energy of the $2p$ orbitals of carbon is indicated by the horizontal line.

The energy of the $4d$ orbitals follows a similar trend with increasing atomic number, with the $4d$ orbitals dropping substantially in energy as the nuclear charge is increased. This stabilization of the $4d$ orbitals is so great that by the end of the $4d$ series the $5s$ orbital is empty in the $4d^{10}$, $^1S$ ground state of atomic Pd.

A comparison of the size of the metal $4d$ and carbon $2p$ orbitals shows that the best match in radial expectation value, $\langle r \rangle$, occurs between Tc and Ru (see Fig. 6). Likewise, a comparison of the orbital energies calculated by numerical Hartree–Fock methods[55] for the $4d^n5s^1$ configurations of the metal atoms and for the $1s^22s^22p^2$, $^3P$ state of the carbon atom, displayed in Fig. 7, shows that the $4d_M$ and $2p_C$ orbitals are most similar in energy when the metal atom is Ru or Rh. These considerations suggest that the best $4d-2p$ bonds will be formed in RuC and its neighboring metal carbides TcC and RhC.

Table VIII provides a list of the ground and low-lying excited electronic states of the $4d$ transition metal carbides, along with bond lengths, vibrational frequencies, and dissociation energies as deduced from experiment.[58–62] For TcC, experimental studies have been understandably few, so values given in square brackets provide the results of a density functional calculation.[44] The prediction of optimal M–C bonding in RuC, based on orbital size and energy effects, is fulfilled surprisingly well in the results presented in this table. Without question, RuC has the shortest bond length, highest vibrational frequency, and greatest dissociation energy of any of the $4d$ transition metal carbides. Moving beyond RuC to RhC, one finds a minor increase in bond length, a decrease in vibrational frequency and a drop in bond energy. These effects are probably related to the occupation of the $12\sigma$ orbital, which is 69% Rh $5s$ in character,[6] and is unoccupied in the ground states of ZrC, NbC, MoC, and RuC. Occupation of this orbital by a single electron is found to increase the bond length and decrease the vibrational frequency in the low-lying excited states of MoC ($[\ldots]2\delta^1 12\sigma^1$, $^3\Delta_2$) and RuC ($[\ldots]2\delta^3 12\sigma^1$, $^3\Delta_3$). Occupation of the $12\sigma$ orbital with two electrons, in the ground $[\ldots]2\delta^4 12\sigma^2$, $^1\Sigma^+$ state of PdC, leads to a significant weakening of the chemical bond. This is apparent from the increase in bond length, decrease in vibrational frequency, and reduction in bond energy for PdC, as compared to the other $4d$ transition metal carbides.

Moving to the lighter transition metal carbides, MoC, NbC, ZrC, and YC, one observes a steady weakening of the chemical bond, with the bond lengths increasing and vibrational frequencies decreasing as one moves to the left across the $4d$ series. Likewise, a steady drop in dissociation energy is also found, with the exception of MoC, which displays an anomalously low bond energy. As has been pointed out by Simard *et al.*,[20] the low bond energy of MoC results from the fact that the MoC $[\ldots]2\delta^2$, $^3\Sigma^-$ ground state cannot dissociate to Mo $4d^55s^1$, $^7S+C2s^22p^2$, $^3P$ ground state atoms. Instead, spin conservation dictates that the MoC ground state must correlate to the Mo $4d^55s^1$, $^5S+C2s^22p^2$, $^3P$ excited separated atom limit, which lies 1.335 eV above ground state atoms. This implies that the promotion-corrected bond energy of MoC, given by $D_0(\mathrm{MoC})+E_p$, where $E_p$ is the Mo promotion energy, is $6.35\pm0.13$ eV. In this context we point out that the paper on NbC by Simard *et al.*[20] erroneously reports the bond energy of MoC as $4.31\pm0.20$ eV, a value which is actually the bond energy of $Mo^+$–C.[58]

Similar modifications are required to obtain the promotion-corrected bond energies of NbC, RuC, and PdC. These transition metal carbides again cannot dissociate to the ground separated atom limits of $^6D+^3P$, $^5F+^3P$, and $^1S+^3P$, respectively, because these limits cannot generate the $^2\Delta_r$, $^1\Sigma^+$, and $^1\Sigma^+$ ground states of these molecules. Adding the spin-orbit averaged promotion energies of 0.184, 0.782, and 0.951 eV to the bond energies of NbC, RuC, and PdC, respectively, we obtain promotion-corrected bond energies of $5.57\pm0.15$, $7.29\pm0.11$, and $<5.41$ eV, respectively. Including these promotion corrections to the bond energy underscores even further the intrinsic strength of the chemical bond in diatomic RuC.

Rather little is experimentally known about TcC, as might be expected. The bond energy has been measured by a Knudsen effusion mass spectrometric investigation,[59] however, and a density functional calculation of its properties has been reported.[44] The theoretical calculation predicts a $[\ldots]2\delta^2 12\sigma^1$, $^4\Sigma^-$ ground state, although this is erroneously stated to be of $^4\Sigma^+$ symmetry in the published article.[44] It is surprising that this state should be the ground state, because it places one electron in the $12\sigma$ orbital. Placement of an electron in this orbital weakens the chemical bond in the low-lying excited states of MoC, RuC, and RhC, as judged by the bond lengths and vibrational frequencies. Instead, one might expect the $[\ldots]2\delta^3$, $^2\Delta_i$ state to be the ground state. Indeed, on the basis of the calculated vibrational frequency and bond length, the $[\ldots]2\delta^3$, $^2\Delta_i$ state of TcC would seem to be more strongly bound than the $[\ldots]2\delta^2 12\sigma^1$, $^4\Sigma^-$ ground state.

The reason that the more weakly bound $[\ldots]2\delta^2 12\sigma^1$, $^4\Sigma^-$ state is calculated to lie below the strongly bound $[\ldots]2\delta^3$, $^2\Delta_i$ state is straightforward. The $[\ldots]2\delta^2 12\sigma^1$, $^4\Sigma^-$ state can dissociate to the ground state separated atom limit of Tc $4d^55s^2$, $^6S+C2s^22p^2$, $^2P$, but the $[\ldots]2\delta^3$, $^2\Delta_i$ state must dissociate to the Tc $4d^65s^1$, $^4D+C2s^22p^2$, $^2P$ excited separated atom limit, 1.368 eV above ground state atoms. Thus the $[\ldots]2\delta^3$, $^2\Delta_i$ state would require a

TABLE VIII. Bonding trends in the $4d$ transition metal carbide.[a]

| Molecule | $D_0$(eV) | Ground state | $r_0$(Å) | $\omega_e$(cm$^{-1}$) | Promotion energy (eV) and promoted metal term | Promotion-corrected bond energy (eV) | Lowest excited state | $T_0$(cm$^{-1}$) | $r_e$(Å) | $\omega_e$(cm$^{-1}$) | Promotion energy (eV) and promoted metal term | Promotion corrected bond energy (eV) |
|---|---|---|---|---|---|---|---|---|---|---|---|---|
| YC | $4.29\pm0.15$[c] | $[\ldots]11\sigma^1 5\pi^3 12\sigma^1$, $^4\Pi_{5/2}$ | 2.050[d] | $686\pm20$[d] | 0.000 $4d^1 5s^2$, $^2D$ | $4.29\pm0.15$ | | | | | | |
| ZrC | $5.1\pm0.4$[e] | $[\ldots]5\pi^4 11\sigma^2 2\delta^0$, $^1\Sigma^+$ | 1.74[f] | $\Delta G_{1/2}=905$[f] | 0.000 $4d^2 5s^2$, $^3F$ | $5.1\pm0.4$ | | | | | | |
| NbC | $5.85\pm0.13$[g] or $5.39\pm0.15$[h] | $[\ldots]2\delta^1 12\sigma^0$, $^2\Delta_{3/2}$ | 1.700[h] | 980[h] | 0.184 $4d^3 5s^2$, $^4F$ | $6.03\pm0.13$ or $5.57\pm0.15$ | $[\ldots]2\delta^0 12\sigma^1$, $^2\Sigma^+$ | 830[h] | [1.729][h] | 980[h] | 0.184 $4d^3 5s^2$, $^4F$ | $5.93\pm0.13$ or $5.47\pm0.15$ |
| MoC | $5.01\pm0.13$[i] | $[\ldots]2\delta^2$, $^3\Sigma^-_{0^+}$ | 1.676[j] | $1008\pm9$[k] | 1.335 $4d^5 5s^1$, $^5S$ | $6.35\pm0.13$ | $[\ldots]2\delta^1 12\sigma^1$, $^3\Delta_2$ | 4002.5[k] | [1.688][i] | 1003[k] | 1.467 $4d^4 5s^2$, $^5D$ | $5.98\pm0.13$ |
| TcC | $6.05\pm0.09$[l] | $[\ldots]2\delta^2 12\sigma^1$, $^4\Sigma^-$ | [1.710][m] | [937][m] | 0.000 $4d^5 5s^2$, $^6S$ | $6.05\pm0.09$ | $[\ldots]2\delta^3$, $^2\Delta_i$ | [2815][m] | [1.663][m] | [1083][m] | 1.368 $4d^6 5s^1$, $^4D$ | $7.07\pm0.09$ |
| RuC | $6.34\pm0.11$[n] | $[\ldots]2\delta^4$, $^1\Sigma^+$ | 1.607[b] | $1100\pm1.5$[k] | 0.782 $4d^8 5s^0$, $^3F$ | $7.12\pm0.11$ | $[\ldots]2\delta^3 12\sigma^1$, $^3\Delta_3$ | 75.953[i] | 1.635[o] | 1038.36[o] | 0.000 $4d^7 5s^1$, $^5F$ | $6.33\pm0.11$ |
| RhC | $5.97\pm0.04$[n] | $[\ldots]2\delta^4 12\sigma^1$, $^2\Sigma^+$ | $r_e=1.613$[q] | 1049.87[q] | 0.000 $4d^8 5s^1$, $^4F$ | $5.97\pm0.04$ | $[\ldots]2\delta^4 6\pi^1$, $^2\Pi_{1/2}$ | 9852.85[q] | 1655[q] | 944.27[q] | 0.000 $4d^8 5s^1$, $^4F$ | $4.75\pm0.04$ |
| PdC | [3.43][r] or $<4.46$[s] | $[\ldots]2\delta^4 12\sigma^2$, $^1\Sigma^+$ | 1.712[t] | $847.6\pm1.6$[k] | 0.951 $4d^9 5s^1$, $^3D$ | [4.38] or $<5.41$ | $[\ldots]12\sigma^1 6\pi^1$, $^3\Pi_{0^-}$ | 2157.1[k] | | $\Delta G_{1/2}=765.1$[k] | 0.000 $4d^{10} 5s^0$, $^1S$ | [3.16] or $<4.19$ |

[a]Numbers in brackets denote theoretical results.
[b]For purposes of this discussion, ''promotion-corrected bond energy'' refers to the energy difference between the ground state and the separated atom limit from which the ground state derives. This differs from the value quoted for $D_0$, which measures the energy difference between the $v=0$ level of the ground state and the lowest separated atom limit, by the promotion energy, $E_p$. $E_p$ is defined as the spin-orbit averaged energy of the promoted atomic term minus the spin-orbit averaged energy of the ground atomic term.
[c]Reference 39.
[d]Reference 19.
[e]Reference 59.
[f]Reference 58.
[g]Reference 60.
[h]Reference 20.
[i]Reference 52.
[j]Reference 13.
[k]This work.
[l]Reference 57.
[m]Reference 44.
[n]Reference 38.
[o]Reference 14.
[p]Reference 61.
[q]Reference 62.
[r]Reference 47.
[s]Reference 41.
[t]Reference 15.

promotion-corrected dissociation energy at least 1.368 eV greater than that of the $[\ldots]2\delta^2 12\sigma^1$, $^4\Sigma^-$ state for it to become the ground state of TcC.

If we accept the calculated energy separation between the $[\ldots]2\delta^2 12\sigma^1$, $^4\Sigma^-$ and $[\ldots]2\delta^3$, $^2\Delta_i$ $v=0$ levels of 2815 $cm^{-1}$, promotion-corrected bond energies for these two states of TcC may be calculated from the Knudsen effusion value of $D_0$(TcC), giving $6.05\pm0.09$ eV and $7.07\pm0.09$ eV, respectively. These values are compared to the promotion-corrected bond energies of the other $4d$ metal carbides in Table VIII. The $[\ldots]2\delta^n 12\sigma^0$ states of ZrC, NbC, MoC, TcC, and RuC display a steady increase in promotion-corrected bond energy as one moves from ZrC to RuC. Similarly smooth trends in decreasing bond length and increasing vibrational frequency are also obtained for the $[\ldots]2\delta^n 12\sigma^0$ states of these molecules, as one moves toward higher atomic numbers.

As listed in Table VIII, smooth trends in the promotion-corrected bond energies, vibrational frequencies, and bond lengths are also obtained for the $[\ldots]2\delta^{n-1}12\sigma^1$ states of NbC, MoC, TcC, RuC, and RhC, except for the calculated values of $\omega_e$ and $r_e$ for the $[\ldots]2\delta^2 12\sigma^1$, $^4\Sigma^-$ state of TcC. The calculated value of $\omega_e$ seems to be about 80 $cm^{-1}$ too small, while the calculated value of $r_e$ seems about 0.05 Å too large. Further experimental or calculational work on TcC would be desirable to clarify these discrepancies.

In comparing the properties of the $[\ldots]2\delta^n$ and $[\ldots]2\delta^{n-1}12\sigma^1$ states of these molecules, the differences in chemical bonding are rather minor for the earlier transition metal carbides, such as NbC and MoC. The promotion-corrected bond energies and vibrational frequencies of the $[\ldots]2\delta^n$ and $[\ldots]2\delta^{n-1}12\sigma^1$ states of these molecules differ by at most 0.37 eV and 16 $cm^{-1}$, respectively. By RuC, however, the $[\ldots]2\delta^4$, $^1\Sigma^+$ state has a promotion-corrected bond energy that exceeds that of the $[\ldots]2\delta^3 12\sigma^1$, $^3\Delta$ state by 0.79 eV, and its vibrational frequency exceeds that of the $[\ldots]2\delta^3 12\sigma^1$, $^3\Delta$ state by 64 $cm^{-1}$. Although the $12\sigma$ orbital remains primarily nonbonding in character, occupation of this orbital becomes progressively more unfavorable as one moves farther to the right in the series of $4d$ transition metal carbides. This probably occurs because this orbital is primarily $5s$ in character, and its occupation prevents the carbon atom from approaching as close as required for optimal overlap with the metal $4d$ electrons. This effect is exacerbated as one moves to the right in the $4d$ series, due to the greater contraction of the $4d$ orbitals as compared to the $5s$ orbital as one moves across the series (see Fig. 6). The exceptionally high vibrational frequency, short bond length, and large promotion-corrected bond energy of the $[\ldots]2\delta^4$, $^1\Sigma^+$ state of RuC all result from the comparable size of the $4d_{Ru}$ and $2p_C$ atomic orbitals, coupled with the fact that neither the $12\sigma$ nonbonding orbital nor the $6\pi$ antibonding orbital is occupied in this state.

## V. CONCLUSIONS

In this work, the results of dispersed fluorescence spectroscopy for three $4d$ transition metal carbides have been presented. The $[\ldots]2\delta^1 12\sigma^1$, $^3\Delta_2$, and $^1\Delta_2$ states of MoC, the $[\ldots]2\delta^3 12\sigma^1$, $^1\Delta_2$ state of RuC, and the $[\ldots]2\delta^4 12\sigma^1 6\pi^1$, $^3\Pi_{0^-}$, $^3\Pi_{0^+}$, $^3\Pi_1$, and $^3\Pi_2$ states of PdC are observed for the first time. In addition, dispersed fluorescence spectroscopy has confirmed the assignment of the $[17.9]^3\Sigma^+(\Omega=1)$ state of PdC, as reported in a previous R2PI study from this group.[15] The observation of the $[\ldots]2\delta^4 12\sigma^1 6\pi^1$, $^3\Pi_\Omega$ states of PdC has allowed the unambiguous identification of the PdC ground state as $[\ldots]2\delta^4 12\sigma^2$, $^1\Sigma^+$. Vibrational frequencies for the ground states of MoC, RuC, and PdC were also measured. In addition, the observed spin-orbit interactions in these molecules have been used to estimate the compositions of electronic states that are mixed by spin-orbit interactions. Similarly, the measured spin-orbit interactions have been used to deduce the compositions of the molecular orbitals in these molecules. The results are in remarkably good agreement with high-level *ab initio* theory. Finally, the trends in bond energy, bond length, and vibrational frequency are examined as one moves across the series of $4d$ transition metal carbides.

## ACKNOWLEDGMENTS

We thank the U.S. Department of Energy for generous support of this research. We also acknowledge the donors of the Petroleum Research Fund, administered by the American Chemical Society, for partial support of this work. R.G.M. acknowledges support from the Undergraduate Research Experience program, administered by the National Science Foundation. We also thank Professor Edward M. Eyring for the generous loan of a Lambda Physik FL2002 Dye Laser that was used in this work.

[1] R. Scullman and B. Thelin, Phys. Scr. **3**, 19 (1971).
[2] R. Scullman and B. Thelin, Phys. Scr. **5**, 201 (1972).
[3] A. Lagerqvist, H. Neuhaus, and R. Scullman, Z. Naturforsch. A **20**, 751 (1965).
[4] A. Lagerqvist and R. Scullman, Ark. Fys. **32**, 475 (1966).
[5] B. Kaving and R. Scullman, J. Mol. Spectrosc. **32**, 475 (1969).
[6] J. M. Brom, Jr., W. R. M. Graham, and W. Weltner, Jr., J. Chem. Phys. **57**, 4116 (1972).
[7] J. H. Hafner, M. J. Bronikowski, B. R. Azamian, P. Nikolaev, A. G. Rinzler, D. T. Colbert, K. A. Smith, and R. E. Smalley, Chem. Phys. Lett. **296**, 195 (1998).
[8] A. W. Castleman, Jr., B. Guo, and S. Wei, Int. J. Mod. Phys. B **6**, 3587 (1992).
[9] B. C. Guo and A. W. Castleman, Jr., Adv. Met. Semicond. Clusters **2**, 137 (1994).
[10] A. W. Castleman, Jr. and B. Guo, Adv. Sci. Technol. (Faenza, Italy) **4**, 125 (1995).
[11] J. S. Pilgrim and M. A. Duncan, Adv. Met. Semicond. Clusters **3**, 181 (1995).
[12] M. A. Duncan, J. Cluster Sci. **8**, 239 (1997).
[13] D. J. Brugh, T. J. Ronningen, and M. D. Morse, J. Chem. Phys. **109**, 7851 (1998).
[14] J. D. Langenberg, R. S. DaBell, L. Shao, D. Dreessen, and M. D. Morse, J. Chem. Phys. **109**, 7863 (1998).
[15] J. D. Langenberg, L. Shao, and M. D. Morse, J. Chem. Phys. **111**, 4077 (1999).
[16] X. Li and L.-S. Wang, J. Chem. Phys. **109**, 5264 (1998).
[17] X. Li, S. S. Liu, W. Chen, and L.-S. Wang, J. Chem. Phys. **111**, 2464 (1999).
[18] A. J. Merer and J. R. D. Peers, in Ohio State 53rd International Symposium on Molecular Spectroscopy, Columbus, OH, 1998, Abstract RI04, p. 249.
[19] B. Simard, P. A. Hackett, and W. J. Balfour, Chem. Phys. Lett. **230**, 103 (1994).
[20] B. Simard, P. I. Presunka, H. P. Loock, A. Bérces, and O. Launila, J. Chem. Phys. **107**, 307 (1997).

[21] Y. M. Hamrick and W. Weltner, Jr., J. Chem. Phys. **94**, 3371 (1991).
[22] R. J. Van Zee, J. J. Bianchini, and W. Weltner, Jr., Chem. Phys. Lett. **127**, 314 (1986).
[23] M. Barnes, A. J. Merer, and G. F. Metha, J. Chem. Phys. **103**, 8360 (1995).
[24] A. G. Adam and J. R. D. Peers, J. Mol. Spectrosc. **181**, 24 (1997).
[25] D. J. Brugh and M. D. Morse, J. Chem. Phys. **107**, 9772 (1997).
[26] M. D. Allen, T. C. Pesch, and L. M. Ziurys, Astrophys. J. **472**, L57 (1996).
[27] W. J. Balfour, J. Cao, C. V. V. Prasad, and C. X. Qian, J. Chem. Phys. **103**, 4046 (1995).
[28] D. J. Brugh and M. D. Morse, unpublished data.
[29] K. Jansson, R. Scullman, and B. Yttermo, Chem. Phys. Lett. **4**, 188 (1969).
[30] K. Jansson and R. Scullman, J. Mol. Spectrosc. **36**, 248 (1970).
[31] K. Jansson and R. Scullman, J. Mol. Spectrosc. **36**, 268 (1970).
[32] A. J. Marr, M. E. Flores, and T. C. Steimle, J. Chem. Phys. **104**, 8183 (1996).
[33] O. Appelblad, R. F. Barrow, and R. Scullman, Proc. Phys. Soc. London **91**, 260 (1967).
[34] O. Appelblad, C. Nilsson, and R. Scullman, Phys. Scr. **7**, 65 (1973).
[35] R. Scullman and B. Yttermo, Ark. Fys. **33**, 231 (1966).
[36] T. C. Steimle, K. Y. Jung, and B.-Z. Li, J. Chem. Phys. **103**, 1767 (1995).
[37] H. Neuhaus, R. Scullman, and B. Yttermo, Z. Naturforsch. A **20**, 162 (1965).
[38] I. Shim, H. C. Finkbeiner, and K. A. Gingerich, J. Phys. Chem. **91**, 3171 (1987).
[39] I. Shim, M. Pelino, and K. A. Gingerich, J. Chem. Phys. **97**, 9240 (1992).
[40] N. Russo, J. Andzelm, and D. R. Salahub, Chem. Phys. **114**, 331 (1987).
[41] I. Shim and K. A. Gingerich, J. Chem. Phys. **76**, 3833 (1982).
[42] I. Shim and K. A. Gingerich, Surf. Sci. **156**, 623 (1985).
[43] H. Tan, D. Dai, and K. Balasubramanian, Chem. Phys. Lett. **286**, 375 (1998).
[44] P. Jackson, G. E. Gadd, D. W. Mackey, H. van der Wall, and G. D. Willett, J. Phys. Chem. A **102**, 8941 (1998).
[45] I. Shim and K. A. Gingerich, Eur. Phys. J. D **7**, 163 (1999).
[46] I. Shim and K. A. Gingerich, Chem. Phys. Lett. **317**, 338 (2000).
[47] I. Shim and K. A. Gingerich, personal communication (1999).
[48] J. C. P. Fabbi, Ph. D., University of Utah, 1995.
[49] S. C. O'Brien, Y. Liu, Q. Zhang, J. R. Heath, F. K. Tittel, R. F. Curl, and R. E. Smalley, J. Chem. Phys. **84**, 4074 (1986).
[50] F. M. Phelps, *Massachusetts Institute of Technology Wavelength Tables* (MIT Press, Cambridge, MA, 1969).
[51] G. Herzberg, *Molecular Spectra and Molecular Structure I. Spectra of Diatomic Molecules*, 2nd ed. (Van Nostrand Reinhold, New York, 1950).
[52] I. Shim and K. A. Gingerich, J. Chem. Phys. **106**, 8093 (1997).
[53] A. G. Adam, Y. Azuma, J. A. Barry, A. J. Merer, U. Sassenberg, J. O. Schröder, G. Cheval, and J. L. Féménias, J. Chem. Phys. **100**, 6240 (1994).
[54] A. M. James, P. Kowalczyk, E. Langlois, M. D. Campbell, A. Ogawa, and B. Simard, J. Chem. Phys. **101**, 4485 (1994).
[55] C. F. Fischer, *The Hartree–Fock Method for Atoms* (Wiley, New York, 1977).
[56] H. Lefebvre-Brion and R. W. Field, *Perturbations in the Spectra of Diatomic Molecules* (Academic, Orlando, 1986).
[57] C. E. Moore, *Atomic Energy Levels*, Natl. Bur. Stand. U.S. Circ. No. 467 (U.S. Government Printing Office, Washington, D.C., 1971).
[58] M. R. Sievers, Y.-M. Chen, and P. B. Armentrout, J. Chem. Phys. **105**, 6322 (1996).
[59] G. H. Rinehart and R. G. Behrens, J. Phys. Chem. **83**, 2052 (1979).
[60] S. K. Gupta and K. A. Gingerich, J. Chem. Phys. **74**, 3584 (1981).
[61] I. Shim and K. A. Gingerich, J. Chem. Phys. **81**, 5937 (1984).
[62] K. P. Huber and G. Herzberg, *Constants of Diatomic Molecules* (Van Nostrand Reinhold, New York, 1979).